Molecular composition and volatility of isoprene photochemical oxidation secondary organic aerosol under low and high NOx conditions

Emma L. D'Ambro[1], Ben H. Lee[2], Jiumeng Liu[3], John E. Shilling[3,4], Cassandra J. Gaston[5], Felipe D. Lopez-Hilfiker[6], Siegfried Schobesberger[2], Rahul A. Zaveri[3], Claudia Mohr[7], Anna Lutz[8], Zhenfa Zhang[9], Avram Gold[9], Jason D. Surratt[9], Jean C. Rivera-Rios[10], Frank N. Keutsch[10], Joel A. Thornton[2]

[1]Department of Chemistry, University of Washington, Seattle, WA, 98195, USA
[2]Department of Atmospheric Sciences, University of Washington, Seattle, WA, 98195, USA
[3]Atmospheric Sciences and Global Change Division, Pacific Northwest National Laboratory, Richland, WA, 99352, USA
[4]Environmental Molecular Sciences Laboratory, Pacific Northwest National Laboratory, Richland, WA, 99352, USA
[5]Rosenstiel School of Marine & Atmospheric Science, University of Miami, FL, 33149, USA
[6]Laboratory of Atmospheric Chemistry, Paul Scherrer Institute, Zurich, Switzerland
[7]Institute of Meteorology and Climate Research, Karlsruhe Institute of Technology, Karlsruhe, Germany
[8]Department of Chemistry, Atmospheric Science, University of Gothenburg, Gothenburg, Sweden
[9]Department of Environmental Sciences and Engineering, Gillings School of Global and Public Health, University of North Carolina, Chapel Hill, NC, 27599, USA
[10]John A. Paulson School of Engineering and Applied Sciences and Department of Chemistry and Chemical Biology, Harvard University, Cambridge, MA, USA

Correspondence to: Joel A. Thornton (thornton@atmos.uw.edu)

Atmospheric
Chemistry
and Physics
Discussions

36 **Abstract.** We present measurements of secondary organic aerosol (SOA) formation from

37 isoprene photochemical oxidation formed in an environmental simulation chamber using dry

38 neutral seed particles, thereby suppressing the role of acid catalyzed multiphase chemistry, at a

39 variety of oxidant conditions. A high-resolution time-of-flight chemical ionization mass

40 spectrometer (HRToF-CIMS) utilizing iodide-adduct ionization coupled to the Filter Inlet for

41 Gases and AEROsols (FIGAERO) allowed for the simultaneous online sampling of the gas and

42 particle composition. Under high HO_2 and low NO conditions, highly oxygenated (O:C $\geq$ 1) C_5

43 compounds were major components (~50%) of the SOA. The overall composition of the SOA

44 evolved both as a function of time and as a function of input NO concentrations. As the level of

45 input NO increased, organic nitrates increased in both the gas- and particle-phases, but the

46 dominant non-nitrate particle-phase components monotonically decreased. We use comparisons

47 of measured and predicted gas-particle partitioning of individual components to assess the

48 validity of literature-based group-contribution methods for estimating saturation vapor

49 concentrations. While there is evidence for equilibrium partitioning being achieved on the

50 chamber residence time scale (5.2 hours) for some individual components, significant errors in

51 group-contribution methods are revealed. In addition, >30% of the SOA mass, detected as low-

52 molecular weight compounds, cannot be reconciled with equilibrium partitioning. These

53 compounds desorb from the FIGAERO at unexpectedly high temperatures given their molecular

54 composition, indicative of thermal decomposition of effectively lower volatility components,

55 likely larger molecular weight oligomers. We use these insights from the laboratory and

56 observations of the same SOA components made during the Southern Oxidant and Aerosol

57 Study (SOAS) to assess the importance of isoprene photooxidation as a local SOA source.

58

Atmospheric
Chemistry
and Physics
Discussions

1   Introduction

Atmospheric aerosol particles reduce visibility, adversely affect human health, and have uncertain overall effects on global climate [*Poschl*, 2005], with particles smaller than 1 µm in diameter playing important roles. Submicron particles typically contain a significant fraction of organic material, on the order of 20-90% [*Jimenez et al.*, 2009; *Zhang et al.*, 2007]. Particulate organic material can be emitted directly to the atmosphere, known as primary organic aerosol, or formed from the gas-to-particle conversion of volatile organic compound (VOC) oxidation products which can partition [*Donahue et al.*, 2011; *Riipinen et al.*, 2011] or react heterogeneously [*Docherty et al.*, 2005; *Gaston et al.*, 2014; *Jang et al.*, 2002; *Surratt et al.*, 2007; *Surratt et al.*, 2006] on existing particles, or homogeneously nucleate to form new particles [*Kirkby et al.*, 2016]. This condensed phase organic material arising from gas to particle conversion is known as secondary organic aerosol (SOA).

Biogenic VOC (BVOC) contribute significantly to SOA. Emitted at rates of 500 TgC/year [*Guenther et al.*, 2012] and with a high reactivity, isoprene (C_5H_8) has the potential to contribute substantially to SOA, even if the overall conversion is inefficient. Initially, the observed products of isoprene oxidation were of high volatility, which led to the hypothesis that isoprene did not generate SOA [*Pandis et al.*, 1991]. However, subsequent chamber experiments showed that the yield of SOA from isoprene photochemical oxidation can range from <1-29% with the highest yields achieved either with acidic aqueous seed particles [*Surratt et al.*, 2010] or as a transient during successive oxidative aging [*Kroll et al.*, 2006]. Chemically speciated measurements of atmospheric aerosol components in an isoprene-rich environment identified polyol compounds likely formed from isoprene oxidation [*Claeys et al.*, 2004; *Paulot et al.*, 2009b]. Subsequent chamber studies have shown that, under low NO conditions, isoprene reacts

Atmospheric
Chemistry
and Physics
Discussions

82   with OH followed by HO_2 to form a hydroxy hydroperoxide, ISOPOOH, which further reacts

83   with OH to form the isoprene epoxy diol, IEPOX [*Paulot et al.*, 2009a; *Paulot et al.*, 2009b].

84   Both laboratory and field studies suggest that IEPOX plays an important role in the formation of

85   isoprene SOA (iSOA) *via* acid catalyzed heterogeneous reactions on deliquesced particles

86   [*Gaston et al.*, 2014; *Lin et al.*, 2013a; *Lin et al.*, 2014; *Lin et al.*, 2012; *Lin et al.*, 2013b; *Liu et*

87   *al.*, 2014; *Nguyen et al.*, 2014; *Paulot et al.*, 2009b; *Surratt et al.*, 2010; *Surratt et al.*, 2006]. In

88   the absence of acidic seed particles, iSOA yields have generally been low, but functional group

89   analyses suggested a significant contribution of peroxide moieties and a complex dependence

90   upon NO_x [*Dommen et al.*, 2006; *King et al.*, 2010; *Kroll et al.*, 2005; 2006; *Sato et al.*, 2011; *Xu*

91   *et al.*, 2014; *Zhang et al.*, 2011]. Despite these advances, a comprehensive molecular

92   characterization of photochemical iSOA has been lacking.

93   Much attention has been focused on the formation of SOA derived from IEPOX

94   chemistry; however, understanding the formation of SOA from pathways other than IEPOX is

95   important for quantifying SOA in environments where the SOA is likely formed via other

96   mechanisms due to the lack of acidic seed. Three recent studies have performed photochemical

97   oxidation on either ISOPOOH [*Krechmer et al.*, 2015; *Riva et al.*, 2016] or both isoprene and

98   ISOPOOH [*Liu*, 2016] in the absence of wet acidic seed in order to study the mechanism of

99   iSOA formation when the IEPOX pathway is suppressed. These studies identified several C_5H_{8-}

100   $_{12}O_{4-8}$ compounds in both the gas- [*Krechmer et al.*, 2015] and particle- [*Liu*, 2016; *Riva et al.*,

101   2016] phases. Liu et al. [2016] found that under the photochemical conditions of their chamber,

102   the most abundant compound in the particle-phase was $C_5H_{12}O_6$, $ISOP(OOH)_2$, presumed to be a

103   dihydroxy dihydroperoxide formed from the reaction of an organic peroxy radical (RO_2) derived

104   from ISOPOOH + OH followed by further reaction with hydroperoxyl radicals (HO_2) [*Liu*,

Atmospheric
Chemistry
and Physics
Discussions

105 2016]. However, the iSOA yields starting from isoprene reported by Liu et al. [2016] were

106 substantially higher than those starting from ISOPOOH alone as reported by Krechmer et al.

107 [2015], and generally higher than most previous iSOA studies in the absence of deliquesced

108 acidic seed particles [*Dommen et al.*, 2006; *King et al.*, 2010; *Xu et al.*, 2014].

109 Furthermore, there is significant interest in understanding how anthropogenic pollutants

110 affect SOA yields [*Shilling et al.*, 2013; *Weber et al.*, 2007; *Xu et al.*, 2015], and there have been

111 several chamber studies to understand the role of NO_x specifically on iSOA yields [*Dommen et*

112 *al.*, 2006; *King et al.*, 2010; *Kroll et al.*, 2005; 2006; *Xu et al.*, 2014; *Zhang et al.*, 2011]. The

113 general effect of NO_x on the newly discovered non-IEPOX SOA system has been described

114 previously [*Liu*, 2016]. The total SOA mass concentration was shown to be stable for input NO

115 concentrations from 0-20 ppb, with a sharp decrease in SOA mass concentration at the highest

116 input NO concentration (50 ppb). While these studies have advanced our knowledge of the

117 possible mechanisms of iSOA formation, in order to more accurately assess the environments in

118 which this pathway will operate, it remains important to further quantify (*a*) the branching

119 between the formation of the $C_5H_{11}O_6$ peroxy radical versus the formation of IEPOX from the

120 reaction between ISOPOOH and OH, (*b*) the fate of the $C_5H_{11}O_6$ peroxy radical under various

121 environmental conditions, as well as (*c*) the volatility of the SOA formed under various

122 environmental conditions and (*d*) the role of the broader suite of oxidation products in the

123 formation of this non-IEPOX SOA.

124 We present laboratory chamber studies of the gas- and particle-phase composition

125 resulting from both the low- and high-NO_x photochemical oxidation of isoprene with the goal of

126 better understanding the chemical mechanisms of iSOA formation and the evolution of its

127 volatility and composition over time, specifically points (*c*) and (*d*) above. We compare the

Atmospheric
Chemistry
and Physics
Discussions

Open Access

EGU

128   observed gas-particle partitioning of several oxidation products to an assumption of equilibrium

129   partitioning theory. In this analysis, we use the measured thermograms of particle-phase

130   components to assess commonly used group-contribution methods for estimating saturation

131   vapor concentrations, C*. Moreover, we use a combined composition-volatility framework

132   [*Lopez-Hilfiker et al.*, 2015] to quantify the presence of more refractory oligomer-like

133   components of the SOA. We compare our laboratory results to ambient measurements taken

134   during the Southern Oxidant and Aerosol Study (SOAS) 2013 field campaign where similar

135   isoprene photochemical SOA tracers were observed. From these analyses we find (*i*) the direct

136   effect of higher NO_x (i.e. all else being constant) is a suppression of iSOA yields at very high

137   input NO concentrations (50 ppb); (*ii*) a large shift to more refractory components and N-

138   containing products with increasing NO_x; (*iii*) a generally important role for accretion reactions

139   and other multiphase chemistry irrespective of NO_x concentrations, even at relatively low

140   precursor concentrations, likely involving a broad suite of isoprene oxidation products.

141

142   2   Experimental methods

143   2.1   Chamber Operation

144   Experiments were performed in the Pacific Northwest National Laboratory's (PNNL) 10.6 m^3

145   polytetrafluoroethylene (PTFE) environmental chamber. The chamber has been described in

146   detail elsewhere [*Liu et al.*, 2012], and a portion of the data discussed herein were obtained from

147   the same experiments described in Liu et al. [2016]. Additional experiments with identical

148   chamber operation were conducted to examine a wider range of oxidant conditions. The chamber

149   was primarily operated in continuous-flow mode where reactants were continuously delivered at

150   a constant rate to allow reaction precursors and products to reach steady state concentrations

Atmospheric
Chemistry
and Physics
Discussions

151   [*Shilling et al.*, 2008]. The extent of reaction is controlled by oxidant concentrations and the

152   residence time of air within the chamber, typically 5.2 hours. We also discuss a time-dependent

153   "batch mode" experiment also performed during 2015 for comparison purposes where the

154   chamber is filled with a fixed amount of isoprene and oxidant precursors in the dark and then the

155   chemistry is followed for ~6 hours after turning on the UV-VIS lights.

156   Isoprene was delivered into the chamber via a calibrated cylinder (Matheson, 20 ppm in

157   nitrogen) and mass flow controller. OH radicals were generated by the photolysis of H_2O_2. An

158   aqueous solution of H_2O_2 was introduced into the chamber via an automated syringe operated at

159   various flow rates to achieve a range of H_2O_2, and therefore OH and HO_2, concentrations.

160   Monodisperse, 50 nm diameter solid ammonium sulfate seed particles were continually added to

161   facilitate the partitioning of oxidized VOC onto particle surfaces as opposed to chamber walls

162   [*Zhang et al.*, 2014] for the formation of SOA. When desired, NO was added via a calibrated

163   cylinder (Matheson, 500 ppm in nitrogen) and mass flow controller. During the continuous-flow

164   experiments RH was controlled to ~50 %, while the batch mode experiment was performed

165   under dry conditions (~10% RH).

166

167   **2.2   Instrumentation**

168   A suite of online instruments were utilized to monitor gas- and particle-phase composition.

169   Ozone and $NO/NO_2/NO_x$ concentrations were measured using commercial instruments (Thermo

170   Environmental Instruments models 49C and 42C, respectively). Aerosol number and volume

171   concentrations were measured with a scanning mobility particle sizer (SMPS). An Aerodyne

172   high-resolution time-of-flight aerosol mass spectrometer (HRToF-AMS) monitored bulk

173   submicron organic and inorganic aerosol composition. The evolution of isoprene was monitored

174   with an Ionicon proton-transfer-reaction mass spectrometer (PTR-MS).

175   A high-resolution time-of-flight chemical ionization mass spectrometer (HRToF-CIMS)

176   using iodide-adduct ionization as described previously [*Lee et al.*, 2014] was coupled to a Filter

177   Inlet for Gases and AEROsols (FIGAERO) [*Lopez-Hilfiker et al.*, 2014] for measuring a suite of

178   oxygenated products in the gas- and particle-phase. The HRToF-CIMS provides measurements

179   of molecular composition, although cannot provide structural information and therefore cannot

180   differentiate between isobaric compounds. Briefly, the FIGAERO is an inlet manifold that

181   allowed for measurement of both gas- and particle-phase molecular composition with

182   approximately hourly time resolution. To collect particles, chamber air was drawn through a 1.27

183   cm OD (2014) or 0.635 cm OD (2015) stainless steel tube at 2.5 slpm across a Teflon filter

184   (Zefluor® 24 mm diameter, 2.0 μm pore size, Pall Corp.) for 31 (2014), 42 (2015), or 25 (batch)

185   minutes. Through a separate inlet chamber air was simultaneously sampled at 22 slpm (2014) or

186   12 slpm (2015) through a 1.9 cm OD, 2 m long (2014) or 1.1 m long (2015) PTFE tube for gas-

187   phase analysis. The gas-phase analysis required sub-sampling a portion of the flow after dilution

188   to maintain linearity of response in the chemical ionization. After a particle collection period,

189   gas-phase analysis ends and the filter containing collected particles is actuated to a location

190   downstream of an ultra-high purity (UHP) N_2 source and immediately upstream of an orifice into

191   the HRToF-CIMS. UHP N_2, continually passed across the filter at 2.5 slpm, was heated at a rate

192   of 10 or 15 °C min^{-1} to 200 °C for a temperature-programed thermal desorption and then kept at

193   200 °C for the remainder of the desorption time (60 min total 2014, 70 min 2015, 40 min batch).

194   The coupled FIGAERO HRToF-CIMS will be referred to herein as the FIGAERO-CIMS. The

195   temperature axis of the FIGAERO thermograms is calibrated with compounds having known

Atmospheric
Chemistry
and Physics
Discussions

196 enthalpies of sublimation [*Lopez-Hilfiker et al.*, 2014]. Lopez-Hilfiker et al. [2014] have shown

197 that pure compounds, or mixtures of non-interacting compounds, have consistent thermogram

198 shapes throughout time and reach a maximum signal at characteristic temperature (T_{max}) which

199 can be related to their enthalpies of sublimation and therefore sub-cooled pure component vapor

200 pressures. In this way, the T_{max} of detected compounds can be used to estimate their C* at

201 ambient conditions even if the structure is unknown.

202

203 **2.3   Experimental Overview**

204 Figure 1 presents a time series of all steady-state experiments. The left and right columns contain

205 experiments conducted in May of 2014 and 2015, respectively. The top panels show the input

206 concentrations of isoprene, hydrogen peroxide, and NO, as well as the isoprene and $C_5H_{10}O_3$

207 (ISOPOOH + IEPOX) concentrations measured at the chamber output. The phrases "input NO",

208 "input H_2O_2", and "input isoprene", refer to the concentration of precursor that would be in the

209 chamber if there were no loss mechanisms except for dilution. For example, in Figure 1, top, the

210 input isoprene (dashed green line) is flat, while the amount of isoprene remaining in the

211 chamber, i.e. what is measured with the PTR-MS (solid green line), varies depending on the

212 chamber chemical environment. Thus, while we state that we input 0-50 ppb NO in the chamber,

213 in reality steady-state NO concentrations in the chamber are much lower for the majority of the

214 chamber residence time, in fact, usually below the detection limit of the NO analyzer due to loss

215 mechanisms such as nitrate formation and wall deposition.

216   The top row of Figure 1 portrays the time series of gas-phase species: input

217 concentrations of isoprene which were generally similar across both years (26 ppbv 2014, 20

218 ppbv 2015), NO, and H_2O_2, as well as gas-phase measurements of the isoprene remaining in the

Atmospheric
Chemistry
and Physics
Discussions

219   chamber and $C_5H_{10}O_3$. As discussed above, the HRToF-CIMS cannot differentiate isobaric

220   compounds and thus $C_5H_{10}O_3$ represents the sum of ISOPOOH and IEPOX. It is important to

221   note that while we are suppressing the uptake of IEPOX into the particle-phase, it is still

222   produced at a yield of about 70-80% [*St Clair et al.*, 2016] from the reaction of ISOPOOH + OH.

223   The middle row shows the organic aerosol (OA) as measured by the AMS with the AMS blanks

224   highlighted in black squares. Steady-state periods for analysis were determined by an

225   unchanging OA concentration over a period of 2 or more hours typically at least 24 hours after

226   an intentional change in experimental conditions. All AMS data here has been multiplied by a

227   factor of 1.5 to correct for particle wall losses. The bottom panels show the time series of a few

228   dominant particle-phase components as measured by the FIGAERO-CIMS: $C_5H_{12}O_6$, $C_5H_{12}O_5$,

229   and $C_5H_{11}NO_7$. The organic nitrate is scaled by a factor of 20 to show its time series on the same

230   scale, although it is near zero when NO is not added to the chamber. The particle-phase

231   FIGAERO data has also been multiplied by a factor of 1.5 to correct for particle wall losses. The

232   grey shaded areas in the left column indicate when there was a chamber cleaning followed by a

233   dark NO_3 + isoprene experiment that is not discussed here. By systematically scanning H_2O_2 and

234   NO concentrations independently, we were able to test the response and composition of the SOA

235   across a range of oxidant conditions, ranging from more pristine to polluted in terms of NO_x

236   concentrations.

237

238   **3   Results & Discussion**

239   **3.1   Effect of NO_x on Major Gas- and Particle-Phase Species**

240   The gas- [*Krechmer et al.*, 2015] and particle-phase [*Liu*, 2016] species detected from isoprene

241   photochemical oxidation when examining the non-IEPOX SOA pathway have been discussed

242   previously. These studies identified several $C_5H_{8-12}O_{4-8}$ compounds, among many others, and the

243   findings presented here are broadly consistent. Figure 2 summarizes all compounds measured as

244   an iodide-adduct in both the gas- (top) and particle- (bottom) phases at both low (left) and high

245   (right) input NO (20 ppb) for average spectra at steady state. The square root of the background

246   subtracted signals were taken to show the dynamic range and then normalized to the maximum

247   signal within each individual plot. Green bars represent organic compounds with formula

248    $C_xH_yO_zI^-$, while blue are organic nitrates (OrgN) with formula $C_xH_yNO_zI^-$. It is possible that

249   dinitrates were measured, but due to their occurrence at masses where non-nitrates would be

250   observed, they are difficult to conclusively identify and thus are not presented here. Major peaks

251   are labeled with letters corresponding to compounds in Table 1. It is important to note that while

252   the same molecular composition may be present in both the gas- and particle-phase, we do not

253   suggest that they all exist as the same structure in each phase, although some likely do. We will

254   discuss this further in later sections.

255   From Figure 2, the two largest signals detected by the FIGAERO-CIMS in the gas-phase

256   at both low and high input NO are CH_2O_2 (presumably formic acid) and $C_5H_{10}O_3$ (presumably

257   the sum of IEPOX and ISOPOOH). With the addition of NO, the CH_2O_2 signal becomes

258   noticeably larger than that of $C_5H_{10}O_3$, likely due to increased fragmentation. Even without

259   adding NO to the chamber there is still a small amount of NO_x present, likely from photolysis of

260   inorganic nitrate on the chamber walls, as we measure non-negligible OrgN concentrations,

261   although the signal is very small relative to organics. The amount of OrgN in the gas-phase

262   increases with increased NO addition as expected. The majority of the OrgN compounds have 5

263   or fewer carbons and no one component dominates the OrgN. Notable signals include for

264   example $C_4H_7NO_5$ and $C_5H_9NO_{5-6}$. The two largest signals detected by the FIGAERO-CIMS in

265   the particle-phase at both low and high input NO are $C_5H_{12}O_6$ and $C_5H_{12}O_5$. Other compounds

266   with the isoprene C_5 backbone but one degree of unsaturation also represent some of the largest

267   signals at low-NO_x, such as $C_5H_{10}O_{4-7}$. As in the gas-phase, no one component dominates the

268   particle-phase OrgN, although one of the strongest signals is $C_5H_{11}NO_7$, the nitrate analogue to

269     $C_5H_{12}O_6$, formed from the same $C_5H_{11}O_6$ peroxy radical. Compounds with the formula

270     $C_5H_{7,9,11}NO_{4-8}$ are all observed in the particle-phase, consistent with field observations from an

271   isoprene-emitting forest during the SOAS campaign [*Lee et al.*, 2016]. For compounds that are

272   detected in the particle-phase, their T_{max} and thermogram shape are also listed in Table 1 and

273   lends information on the nature of these compounds which will be discussed in further detail

274   later on.

275   The general effect of NO_x on the SOA in this system has been described previously [*Liu*,

276   2016]. Here we highlight the effect of input NO concentrations on individual compounds by

277   focusing on three of the most prominent particle-phase species (Fig. 3, top). As the input NO

278   concentration increases, $C_5H_{12}O_6$ and $C_5H_{12}O_5$ decrease nonlinearly. $C_5H_{11}NO_7$, presumably

279   produced from the ISOPOOH + OH $C_5H_{11}O_6$ peroxy radical increases initially with increasing

280   NO addition. Above moderate NO input (>10 ppb), $C_5H_{11}NO_7$, a nitrate, begins to decrease with

281   further increases in NO addition, likely a result of ISOPOOH also decreasing as the $C_5H_9O_3$

282   peroxy radical reacts more with NO as opposed to HO_2. This behavior supports previous

283   observations of low isoprene SOA yields at high NO_x [*Kroll et al.*, 2005; 2006; *Lane et al.*, 2008;

284   *Xu et al.*, 2014; *Zhang et al.*, 2011], though we note a monotonic NO_x dependence of SOA yield

285   in our experiments. The bottom panel of Figure 3 depicts the mass fraction of OrgN as a function

286   of input NO. The mass fraction of OrgN increases rapidly between 0 and 10 ppb NO input and

287   more modestly above that. At the highest input NO concentration, OrgN make up ~40% of the

Atmospheric
Chemistry
and Physics
Discussions

288   organic aerosol mass detected by the FIGAERO-CIMS. This estimate carries uncertainty due to

289   the inability to calibrate to every OrgN compound, as well as a lack of a single dominant OrgN.

290   At the highest input NO, the AMS measurements also indicate that OrgN make up ~40% of the

291   SOA mass, assuming a molecular weight of the typical OrgN of 148 g/mol based on the

292   measured FIGAERO-CIMS particle-phase OrgN distribution, which is consistent with our

293   findings. Though considerable uncertainties exist with respect to quantification of OrgN using

294   both the AMS and the FIGAERO-CIMS, the agreement between these independent

295   measurements suggests the calibration factors applied to the FIGAERO-CIMS OrgN signals are

296   reasonable. We draw two main conclusions from this analysis: (1) the complementary increase in

297   OrgN and decrease in non-nitrates likely accounts for the stable SOA mass yields at lower input

298   NO concentrations as reported previously [*Liu*, 2016], with the highest input NO concentrations

299   resulting in a decrease in both OrgN and non-nitrates, corresponding to the sharp decrease in

300   SOA mass yield at the highest input NO concentration (50 ppb), and (2) while there is no one

301   OrgN that is most prominent in the gas or particle phase, the total OrgN can compose up to 40%

302   of the SOA mass at high input NO concentrations (50 ppb).

303

3.2   Time Evolution of Low NO_x Isoprene SOA Composition

305   To examine how isoprene photochemical SOA evolves over time, a time-dependent experiment

306   was conducted (Fig. 4) similar to a previous batch mode study [*Kroll et al.*, 2006]. In this "batch

307   mode" experiment, isoprene, H_2O_2, and solid ammonium sulfate seed were injected into the

308   chamber, and then the lights were turned on. The chemistry of the closed system was allowed to

309   evolve in time without further input of reactants. Each pie chart represents a FIGAERO-CIMS

310   particle-phase desorption measurement over the course of the experiment. The data is converted

Atmospheric
Chemistry
and Physics
Discussions

311   to mass concentration as discussed previously [*Lee et al.*, 2014; *Liu*, 2016], the overall size of

312   each pie chart is proportional to the amount of AMS measured OA (9.8, 15.0, 14.8, 14.6 µg/m^3

313   from left to right, corrected for particle wall loss), and the time is the mid-point of the particle

314   collection period (which lasted 25 minutes) relative to the initiation of the chemistry. The

315   desorption just prior to the isoprene injection is used as the baseline, and the corresponding mass

316   spectra are subtracted from the succeeding desorptions. Unlike the work of Kroll et al. [2006]

317   who saw SOA volume maximize after ~3-4 hours of oxidation followed by a large decrease in

318   total volume attributed to photochemical processing, the measurements presented here did not

319   follow the reaction progress long after the maximum OA concentration was achieved (<1 hour)

320   and thus we did not observe a significant decrease in mass.

321   The absolute and relative concentration of $C_5H_{12}O_6$ in the particle-phase decreases from

322   50% of the particle-phase SOA to 25% over the four hours of oxidation. The absolute mass of

323   SOA also changes, primarily increasing, during the experiment, reaching a peak of 15.8 µg/m^3 at

324   t=4.3 hours. This suggests $C_5H_{12}O_6$ is transforming either within the particle-phase via

325   hydrolysis or other mechanisms, or in the gas-phase, with efficient gas-particle equilibration, due

326   to reaction with OH or photolysis [*Baasandorj et al.*, 2010; *Hsieh et al.*, 2014; *Roehl et al.*,

327   2007]. Gas-phase oxidation seems unlikely given that typically greater than 95% of the $C_5H_{12}O_6$

328   is found in the particle-phase (shown below, Fig. 5) when OA > 2 µg/m^3. While many of the

329   detected compounds are present at constant mass fractions throughout time, $C_5H_{12}O_5$, $C_5H_{12}O_4$,

330   and $C_5H_{10}O_3$ increase. $C_5H_{12}O_5$ has been observed previously in the gas-phase from ISOPOOH

331   oxidation [*Krechmer et al.*, 2015], and was also shown to be a large fraction of the particle-phase

332   from isoprene oxidation [*Liu*, 2016], but its production mechanism is uncertain. Krechmer et al.

333   [2015] suggest it could be formed from the oxidation of an impurity in the ISOPOOH, although

Atmospheric
Chemistry
and Physics
Discussions

334   the experiments presented here use isoprene as the BVOC precursor, ruling out this explanation.

335   In these experiments, $C_5H_{12}O_5$ is observed within the first hour of isoprene oxidation and grows

336   to ~25% of the OA mass within 1.5 hours, becoming relatively stable thereafter. One possible

337   source of this compound is $RO_2 + RO_2$ reactions of the ISOPOOH derived peroxy radical and

338   peroxy radicals from a dihydroxy alkene reacting with HO_2. It is also possible that it could be

339   formed in the condensed phase from hydrolysis reactions. Further work is required to understand

340   the source of this compound.

341   The other two compounds that increase with time, $C_5H_{12}O_4$ and $C_5H_{10}O_3$, likely isomers

342   of 2-methyl tetrols and alkene triols respectively, are traditional markers of IEPOX derived SOA

343   [*Claeys et al.*, 2004; *Ding et al.*, 2008; *Edney et al.*, 2005; *Kourtchev et al.*, 2005; *Surratt et al.*,

344   2010; *Xia and Hopke*, 2006]. This result is unexpected given that using effloresced (solid)

345   ammonium sulfate seed at a RH below the deliquescence point (RH ~50%) together with an

346   SOA coating should strongly suppress the known acid catalyzed IEPOX multiphase chemistry

347   [*Gaston et al.*, 2014; *Lin et al.*, 2013a; *Lin et al.*, 2014; *Lin et al.*, 2012; *Lin et al.*, 2013b; *Liu et*

348   *al.*, 2014; *Nguyen et al.*, 2014; *Paulot et al.*, 2009b; *Surratt et al.*, 2010; *Surratt et al.*, 2006]. We

349   tested the uptake of an authentic IEPOX standard onto dry, crystalline ammonium sulfate seed

350   under conditions similar to these, though during continuous-flow mode, and found no

351   measurable uptake and SOA formation [*Liu*, 2016]. However, it is consistent with previous work

352   that found both of these tracers in the SOA when isoprene was oxidized in the absence of

353   deliquesced acidic seed [*Edney et al.*, 2005; *Kleindienst et al.*, 2009]. $C_5H_{12}O_4$ and $C_5H_{10}O_3$ are

354   less than 1% of the SOA for the first 2 hours and then gradually increase to 14% and 8% of the

355   SOA, respectively, after 4 hours. Interestingly, the FIGAERO thermograms for these tracers

356   have broad maxima at much higher T_{max} than would be consistent with their elemental

Atmospheric
Chemistry
and Physics
Discussions

357   composition. Lopez-Hilfiker et al. [2016b] noted two modes in the thermogram of $C_5H_{12}O_4$, one

358   with a T_{max} as expected based on its structure and another with a higher T_{max} indicating an

359   effectively lower volatility component thermally decomposing. The chemical mechanism leading

360   to the desorption of these tracers is unknown, but given that the experimental conditions strongly

361   suppressed the traditional acid catalyzed aqueous IEPOX chemistry, perhaps these tracers are not

362   solely derived from aqueous IEPOX chemistry but isoprene photochemical oxidation more

363   generally. In conclusion, $C_5H_{12}O_6$ condenses rapidly and initially makes up a majority of the

364   SOA mass, but over time its contribution decreases as other compounds such as $C_5H_{12}O_5$,

365    $C_5H_{12}O_4$, and $C_5H_{10}O_3$ increase. While our data suggests these compounds may be formed in the

366   particle phase from heterogeneous reactions, more work is required to determine their sources.

367

368   **3.3   Gas-particle Partitioning: Saturation Vapor Concentrations and Oligomeric**

369   **Content**

370   The volatility of the products generated from the non-IEPOX $C_5H_{12}O_6$ pathway [*Krechmer et al.*,

371   2015; *Liu*, 2016; *Riva et al.*, 2016] will be a crucial aspect of its contribution to SOA formation

372   and the lifetime of the resulting SOA against dilution, gas-phase oxidation, and depositional

373   losses. The capability of the FIGAERO to measure the concentration of individual species in

374   both the gas- and particle-phase allows for a direct measurement of the particle-phase fraction

375   (F_p), which is the particle-phase concentration relative to the gas- and particle-phase

376   concentrations per volume of air. The F_p can also be calculated from an assumption of

377   equilibrium absorptive partitioning theory first described by Pankow [1994] using equation 1,

378   where C* is the saturation vapor concentration ($\mu g/m^3$) of the pure substance and C_{OA} is the

379   concentration of organic aerosol ($\mu g/m^3$).

380 $$F_p = \left(1 + \frac{C^*}{C_{OA}}\right)^{-1} \qquad (1)$$

381 Equation 1 neglects the activity coefficient and molecular weight differences for simplicity,

382 though any C^* derived from a comparison to equation 1 would implicitly include these factors.

383 Calibration standards do not exist for a vast majority of compounds in SOA and therefore the C^*

384 are largely unknown, mitigating somewhat the impact of such simplifications. Group-

385 contribution methods exist to estimate C^*, where each functional group represents a discrete,

386 empirically determined contribution to the equilibrium vapor pressure of a compound [*Capouet*

387 *and Muller*, 2006; *Compernolle et al.*, 2011; *Nannoolal et al.*, 2008; *Pankow and Asher*, 2008].

388 These approaches carry substantial uncertainty for atmospheric SOA systems, in large part due to

389 the lack of enough standards to develop a robust parameterization. In addition, these approaches

390 do not directly address the potential of functional group interactions, such as intramolecular

391 hydrogen bonding, which when not included can lead to C^* estimates that are significantly

392 biased low [*Kurten et al.*, 2016].

393   Measured F_p were determined using the FIGAERO-CIMS for a subset of major particle-

394 phase components from 2015 (Fig. 5). These estimates include the uncertainty associated with

395 differences in inlet and chamber wall losses of vapors relative to particles. Operating the

396 chamber in continuous flow mode likely reduces the impact of chamber walls, at least for low

397 volatility to semi volatile compounds, as some degree of equilibration can occur [*Liu*, 2016;

398 *Shilling et al.*, 2008]. A short (1-2 m) laminar flow Teflon inlet line with a short residence time

399 (<1 s) was coupled to the chamber for the detection of gases by the FIGAERO-CIMS. The

400 diffusion-controlled loss of gases in the tubing is likely less than 50% at most, again a small

401 effect on the comparison of measured and predicted F_p as we will show below.

402   F_p were predicted using equation 1 with C* calculated via the EVAPORATION group-

403   contribution method [*Compernolle et al.*, 2011], which generally gave similar estimates as the

404   Capouet and Muller approach [2006]. The Nannoolal method [2008] was also explored, but it

405   gave C* estimates that varied by several orders of magnitude for structurally similar compounds,

406   as well as estimates that were unexpectedly low based on FIGAERO measurements and what

407   one would expect based on molecular structure, consistent with previous findings [*Kurten et al.*,

408   2016]. The SIMPOL method of Pankow and Asher [2008] was also applied to select compounds

409   and is discussed below. A major limitation of this analysis is that we do not know the structure of

410   the molecules detected, only the elemental composition, and so we make assumptions based on

411   the most likely functional groups expected from the chemical conditions of the chamber and

412   from the elemental composition (e.g., degrees of unsaturation, oxygen to carbon ratio). In many

413   cases these assumptions have little impact on our conclusions.

414   If the SOA formed according to equilibrium partitioning theory as first described by

415   Pankow [1994], the F_p measured by the FIGAERO and the C* calculated using group-

416   contribution methods should be in agreement over a range of organic aerosol mass

417   concentrations. Figure 5 indicates two immediate challenges to testing partitioning theory. First,

418   a large number of mostly small carbon number compounds have a much higher measured F_p

419   relative to the predicted F_p based on their group-contribution determined C*. The C* estimates

420   would have to be in error by at least five or more orders of magnitude, which is likely not the

421   case as there are many measurements of vapor pressures for similar compounds. Furthermore,

422   the thermograms of these compounds appear broad, not Gaussian as one would expect for

423   individual non-interacting compounds [*Lopez-Hilfiker et al.*, 2014], and do not peak until ~85 °C

424   or higher, see Table 1, which is also inconsistent with the calibrated composition-enthalpy of

Atmospheric
Chemistry
and Physics
Discussions

425   sublimation relationship scaled for the FIGAERO used here [*Lopez-Hilfiker et al.*, 2014]. We

426   attribute this behavior to thermal decomposition of lower volatility components during the

427   desorption process giving rise to smaller molecular weight, more volatile components as in

428   previous studies of IEPOX SOA tracers in the southeast U.S. [*Lopez-Hilfiker et al.*, 2016b], α-

429   pinene derived chamber SOA [*Lopez-Hilfiker et al.*, 2015], and biomass burning organic aerosol

430   in the northwest U.S. [*Gaston et al.*, 2016]. That is, the disagreement between measured and

431   predicted F_p for these compounds is not necessarily a failure of equilibrium partitioning theory,

432   nor evidence that equilibrium had not been achieved, but rather that the compounds desorbing

433   were actually part of another larger molecular weight accretion product, the C* and gas-phase

434   concentrations of which are unknown.

435   The second challenge to testing gas-particle partitioning is illustrated in the F_p for two

436   representative compounds, $C_5H_{12}O_6$ and $C_5H_{10}O_6$ (Fig. 5, bottom panels). That there is

437   reasonable agreement between measured and predicted F_p (Fig. 5, bottom right, circles) for

438    $C_5H_{10}O_6$ suggests that equilibrium partitioning is potentially achieved in the chamber. However,

439   that $C_5H_{12}O_6$ is not in good agreement (Fig. 5, bottom left, circles) cannot be explained by

440   thermal decomposition of lower volatility material, because the thermogram shape is Gaussian

441   and therefore looks like a pure component and the predicted F_p is much larger than measured

442   (opposite to the above situation). This behavior implies inaccurate C* derived from the group-

443   contribution methods.

444   The EVAPORATION group-contribution method [*Compernolle et al.*, 2011] used in

445   Figure 5 and that of Capouet and Muller [2006] both produce a C* of 0.03 µg/m^3 for $C_5H_{12}O_6$

446   when assuming it is a dihydroxy dihydroperoxide, while the SIMPOL method predicts 2 µg/m^3

447   [*Pankow and Asher*, 2008]. For $C_5H_{10}O_6$, assumed to be a hydroxy dihydroperoxy aldehyde,

Atmospheric
Chemistry
and Physics
Discussions

Open Access

EGU

448   EVAPORATION [*Compernolle et al.*, 2011] predicts 4 µg/m^3, the Capouet and Muller [2006]

449   method predicts 2 µg/m^3, and SIMPOL [*Pankow and Asher*, 2008] suggests 15 µg/m^3. That the

450    $C_5H_{12}O_6$ values vary by 2 orders of magnitude while the $C_5H_{10}O_6$ values vary by a factor of 7

451   suggests the need for better experimental constraints. Using the measured T_{max} from the

452   FIGAERO thermograms, the C* for $C_5H_{12}O_6$ and $C_5H_{10}O_6$ were determined to be 0.7 and 6.7

453   µg/m^3, respectively. These values were then used to re-calculate the predicted F_p using equation

454   1. The original group-contribution calculated F_p is shown alongside the adjusted points in the

455   bottom panels of Figure 5 as navy crosses. The root mean square error of both $C_5H_{12}O_6$ and

456    $C_5H_{10}O_6$ is minimized when comparing the measurements with the adjusted F_p, indicating that

457   the calibrated FIGAERO temperature axis can more accurately determine the C*.

458   In the case of $C_5H_{12}O_6$ the FIGAERO determined C* is much closer to the SIMPOL

459   estimation, and significantly higher than that estimated by the other group-contribution methods.

460   We suspect the large differences between measured and group-contribution method estimates of

461   C* in this case are due to the lack of vapor pressure data on compounds with hydroperoxide

462   groups, specifically multifunction hydroperoxides: there is only data on four hydroperoxide

463   containing compounds on which these models are based [*Capouet and Muller*, 2006;

464   *Compernolle et al.*, 2011]. It can be argued that -OH and –OOH groups will lower the C*

465   relative to the precursor by a comparable amount, with the possibility that a -OOH group could

466   lower it slightly more due to its additional oxygen. For example, the C* of 2-methyl-1,2,3,4-

467   butanol ($C_5H_{12}O_4$) was calculated to be 9 to 34 µg/m^3, depending on the method used [*Capouet

468   *and Muller*, 2006; *Compernolle et al.*, 2011], roughly 250-1000 times greater than the C*

469   estimates for $C_5H_{12}O_6$. That is, a molecule with the same number of distinct –OH containing

470   functional groups is predicted to have a very different C* because the vapor pressure lowering of

Atmospheric
Chemistry
and Physics
Discussions

471 –OOH groups assumed by these group-contribution methods is larger than that for an -OH

472 group. Our observations suggest this assumption is likely incorrect, at least to the extent

473 employed in these methods, and is supported by previous work that found group-contribution

474 methods predicted significantly lower C* than models did for compounds with multiple

475 functionalities [*Kurten et al.*, 2016; *Valorso et al.*, 2011]. Conversely, we assume $C_5H_{10}O_6$ is a

476 hydroxy dihydroperoxy aldehyde, also with two –OOH groups, but the group contribution

477 methods accurately predicte a C* consistent with that inferred from the FIGAERO T_{max}. This

478 agreement may be a coincidence or indicative of the fact that multifunctional compounds with

479 slightly different function groups can have significantly different intramolecular interactions,

480 leading to significantly different saturation vapor concentrations [*Compernolle et al.*, 2011].

481   There are two main conclusions we draw from Figure 5. The first is that testing

482 equilibrium partitioning theory is a challenge without a direct constraint on the C* like the

483 FIGAERO desorption T_{max} due to possibly large systematic errors in the C* predicted from

484 group-contribution methods. Moreover, thermal decomposition of higher molecular weight

485 compounds, such as oligomers, into smaller molecular weight compounds generates uncertainty

486 in the measured F_p in that the FIGAERO T_{max} derived C* does not correspond in such cases to

487 the observed molecule. From this result we draw our second conclusion: a surprisingly large

488 fraction of the iSOA is resistant to evaporation, indicating it will have a longer lifetime against

489 dilution [*Kroll et al.*, 2006]. Approximately 30-45% of the SOA mass detected by the

490 FIAGERO-CIMS desorbs at temperatures greater than 80 °C, much of that above 100 °C, which

491 corresponds to effective enthalpies of sublimation >150 kJ/mol in our FIGAERO assuming no

492 diffusion limitations to evaporation from the particles that exist at these temperatures (for

493 example, due to highly viscous phases). We note that Kroll et al. [2006] also found evidence for

Atmospheric
Chemistry
and Physics
Discussions

494   a significant mass fraction of large molecular weight compounds when applying the AMS to

495   low-NO_x, non-IEPOX iSOA. We conclude that accretion products are the cause of this more

496   refractory SOA component, but, we cannot determine from the thermograms alone whether the

497   accretion process is reversible at ambient temperatures on longer timescales than the ~1 hour

498   desorptions. That the SOA yield from isoprene is significantly higher for similar organic mass

499   loadings than that reported from ISOPOOH only, suggests an important role for the broader

500   distribution of oxidation products formed in addition to those from ISOPOOH. One possible

501   reason is that these mostly semi volatile products can contribute to lower volatility products via

502   accretion chemistry [*Jathar et al.*, 2016; *Sato et al.*, 2011; *Tsai et al.*, 2015].

503

504   **3.4   Role of NO_x in iSOA volatility**

505   Previous studies using thermal denuders and either an AMS or a tandem differential mobility

506   measurement of particle size distributions have found that iSOA formed in the presence of NO_x

507   is less volatile relative to that formed in HO_2-dominant regimes [*Kleindienst et al.*, 2009; *Xu et*

508   *al.*, 2014]. We compare the iSOA volatility under different regimes by summing the FIGAERO

509   thermogram signals across all ions having formulae $C_xH_yO_zN_{0-1}I^-$. These sum thermograms are

510   plotted as a function of temperature for both low- and high-NO_x conditions in Figure 6, bottom

511   left and right, respectively. Since $C_5H_{12}O_6$ is a large portion of the SOA mass concentration in

512   these experiments (e.g. Fig. 4), it is shown separately in dark green with the remainder of the

513   summed signal shown in light green. $C_5H_{12}O_6$ is clearly a large contribution to the sum signal in

514   both the low- and high-NO_x cases, although more so in the low NO_x regime, with the remaining

515   thermogram signal primarily located in the lower volatility (higher temperature) "tail" of the

516   desorption. At high NO_x, there are two clear modes in the thermogram remaining after removing

Atmospheric
Chemistry
and Physics

Discussions

517   the $C_5H_{12}O_6$ contribution (light green), one mode at roughly the same T_{max}, and therefore

518   volatility, of $C_5H_{12}O_6$, and the other mode at a higher T_{max}, ~110 °C, suggesting a larger fraction

519   of detected iSOA mass at high NO_x is resistant to evaporation compared to the low NO_x case.

520   We also note that the T_{max} of individual compounds shifts to higher values with the addition of

521   NO_x except for the highest mass compounds (see Table 1). Although the thermograms for many

522   of these compounds do not have a distinct Gaussian shape, making determination of the T_{max}

523   uncertain or undefined, the shift to higher T_{max} for the same compounds could indicate not just

524   lower volatility products in the form of oligomers, but also potentially a change in the overall

525   particle viscosity causing the iSOA to be more resistant to evaporation with the addition of NO_x.

526   A sum thermogram of α-pinene ozonolysis that has been previously reported [*Lopez-*

527   *Hilfiker et al.*, 2015] is displayed alongside those of the low- and high-NO_x experiments (Fig. 6,

528   top) for comparison. The α-pinene SOA has a bimodal sum thermogram, similar to that of the

529   high-NO_x iSOA with the second lower volatility modes in the same temperature range. The

530   higher volatility mode of the α-pinene SOA corresponds in temperature space to that of the

531   higher volatility mode of the low-NO_x iSOA. The multiple modes of the α-pinene sum

532   thermogram have the same relative maxima in signal space, unlike the isoprene sum

533   thermograms. α-Pinene ozonlysis apparently generates a larger fraction of lower volatility SOA

534   relative to isoprene photochemical oxidation, although isoprene photochemical SOA has

535   components in the same volatility ranges of α-pinene ozonlysis SOA, and the relative size of the

536   various modes and location in temperature space is dependent on the amount of NO_x.

537   It is important to note that the contribution of the effectively lower volatility components

538   inferred from thermograms in Figure 6 is likely underestimated in both the low- and high- NO_x

539   cases because the thermograms are presented as ion signal space, not mass concentration. If we

Atmospheric
Chemistry
and Physics
Discussions

Open Access

540 converted into mass concentration units prior to calculating the summed thermogram, the

541 contribution of $C_5H_{12}O_6$ would be significantly less than implied in Figure 6. The integrated

542 contribution of $C_5H_{12}O_6$ would instead be more similar to that shown in Figure 4 for which we

543 applied calibration estimates based on ISOPOOH and a range of other oxygenated compounds,

544 together with the ion-molecule collision limited sensitivity discussed previously [*Liu*, 2016;

545 *Lopez-Hilfiker et al.*, 2016a]. In conclusion, the low-NO$_x$ SOA has an overall higher volatility

546 and the addition of NO$_x$ results in lower volatility material making up a larger fraction of the

547 SOA, although the total SOA yield is lower [*Liu*, 2016], in general agreement with previous

548 studies showing that increasing NO$_x$ leads to lower volatility SOA [*Kleindienst et al.*, 2009],

549 likely by enhancing oligomerization [*Dommen et al.*, 2006; *Xu et al.*, 2014]. However, many of

550 these previous studies were carried out in very different concentration regimes with different

551 detection techniques, so that the data we present offers an additional contribution to the general

552 importance of oligomerization.

553

554 **3.5   Comparisons to Ambient SOA Formed in an Isoprene-Rich Environment**

555   During the summer of 2013, the Southern Oxidant and Aerosol Study (SOAS) was

556 conducted in Brent, AL, as described previously [*Attwood et al.*, 2014; *Lee et al.*, 2016;

557 *Washenfelder et al.*, 2015]. The same instrument was used here and for the PNNL chamber

558 studies described herein, allowing for a direct comparison between chamber and field

559 measurements. Due to the influence of anthropogenic sulfur emissions and the high relative

560 humidity, IEPOX multiphase chemistry contributed significantly to SOA in this region as

561 expected [*Budisulistiorini et al.*, 2015; *Hu et al.*, 2015; *Lopez-Hilfiker et al.*, 2016b]. However,

562 we also detected in the ambient SOA the dominant components of the chamber generated SOA

Atmospheric
Chemistry
and Physics
Discussions

563   described above, namely $C_5H_{12}O_6$, $C_5H_{12}O_5$, $C_5H_{11}NO_7$, $C_5H_{10}O_6$, and $C_5H_{10}O_5$, the individual

564   diurnal profiles and the sum of all 5 are shown in Figure 7, bottom. While the FIGAERO-CIMS

565   provides molecular composition and not structural information, that the $C_5H_{12}O_6$ thermograms at

566   SOAS and PNNL look nearly identical and have the same T_{max} (Fig. 7, top) provides some

567   support that the same compounds are present in both systems.

568   The mean diurnal cycle of the sum of the C_5 tracers detected in the PNNL chamber

569   exhibit a daytime maximum (Fig. 7) as expected given the strong daily modulation in isoprene

570   emissions [*Davison et al.*, 2009; *de Arellano et al.*, 2011; *Fuentes et al.*, 1999; *Holzinger et al.*,

571   2002; *Kalogridis et al.*, 2014; *Lee and Wang*, 2006; *Rinne et al.*, 2002; *Yang et al.*, 2005]. The

572   sum of the 5 tracers, $C_5H_{12}O_6$, $C_5H_{12}O_5$, $C_5H_{11}NO_7$, $C_5H_{10}O_6$, and $C_5H_{10}O_5$, reaches a minimum

573   of 40 ng/m^3 during dark hours and a maximum of 90 ng/m^3 during the day (Fig. 7). While similar

574   compounds were measured during SOAS and the PNNL isoprene oxidation experiments,

575   comparisons with field data provides interesting insight into the production of $C_5H_{12}O_5$. Figure 4

576   indicates that the $C_5H_{12}O_5$ SOA mass fraction increases with time relative to $C_5H_{12}O_6$, but

577   saturates at ~20%, and the concentration of $C_5H_{12}O_6$ is always greater than $C_5H_{12}O_5$ in the

578   chamber experiments. In the SOAS field data however, the relationship is reversed: the $C_5H_{12}O_5$

579   is always greater than the $C_5H_{12}O_6$. Although the two are correlated in the chamber ($R^2 = 0.6$),

580   they are not correlated in the atmosphere ($R^2 = 0.1$). While we do not have a definitive

581   explanation, this behavior may be due to a variety of factors. As noted above, the $C_5H_{12}O_5$ could

582   be produced by gas-phase RO_2 + RO_2 chemistry, however, we expect this pathway is more

583   important in the chamber with higher RO_2 concentrations than in the atmosphere. While also

584   possibly tied generally to aging as shown in Figure 4, it could be that multiphase processes such

585   as hydrolysis of hydroperoxides or organosulfate formation and subsequent hydrolysis are more

Atmospheric
Chemistry
and Physics
Discussions

586   significant in ambient particles. That is, assuming $RO_2 + RO_2$ chemistry is less efficient in the

587   ambient atmosphere, a reasonable explanation is that $C_5H_{12}O_5$ represents a hydrolysis product of

588   the dihydroxy dihydroperoxide, $C_5H_{12}O_6$, or related organosulfates, as suggested in the recent

589   work of Riva et al. [2016] and that these processes are enhanced in the aqueous aerosols likely

590   present in the SE U.S.

591

592   **4   Conclusions**

593   We have explored the composition and volatility of isoprene SOA at low and high NO_x

594   concentrations utilizing effloresced ammonium sulfate seed to prevent IEPOX uptake and thus

595   suppress IEPOX multiphase chemistry. We measured compositions of products reported in

596   previous works of similar experiments [*Krechmer et al.*, 2015; *Liu*, 2016], in particular $C_5H_{12}O_6$

597   and related highly oxidized compounds. We examined the saturation vapor concentrations of

598   several of the most dominant particle-phase signals and tested the accuracy of various group-

599   contribution methods to determine the C*. Of the three group-contribution methods assessed, the

600   SIMPOL approach [*Pankow and Asher*, 2008] gave the closest estimates of C* compared to

601   those determined from the thermograms. The vapor pressure lowering effect of –OOH groups,

602   assumed to be abundantly present in this system, appears to be greatly overestimated in two

603   commonly used methods [*Capouet and Muller*, 2006; *Compernolle et al.*, 2011]. Through these

604   analyses we found that a significant fraction of SOA components we measure are likely thermal

605   decomposition fragments, characterized by broad thermograms and higher than expected T_{max}.

606   That such a large fraction (30-45%) of the non-IEPOX iSOA is of low volatility implies

607   the lifetime of non-IEPOX iSOA is longer than would previously be expected. Our findings also

608   suggest that experiments which assess the SOA formation potential of isoprene likely

Atmospheric
Chemistry
and Physics
Discussions

609   underestimate the overall potential due to the participation of a broad suite of products in

610   accretion chemistry. Further work on the role of accretion chemistry in this system is needed to

611   verify that the higher iSOA yield observed by Liu et al. [2016] from isoprene is indeed caused by

612   semi volatile products participating in accretion reactions. Furthermore, we have shown here that

613   the addition of NO has a strong effect on the amount of $C_5H_{12}O_6$ produced, and while the overall

614   volatility of the OA decreases with NO_x, the total amount of OA also decreases [*Liu*, 2016],

615   indicating that in polluted regions the amount of SOA formed from this pathway will be

616   diminished, but the SOA will be longer lived against dilution. In conclusion, due to the high

617   yield of IEPOX from ISOPOOH + OH it has been assumed to be the most important pathway for

618   the formation of iSOA, however, its relatively high volatility (1,1691 μg/m^3 [*Compernolle et al.*,

619   2011]) and the fact that it requires such specific conditions to form SOA efficiently implies that

620   the formation of SOA from the non-IEPOX pathway discussed herein can also play an important

621   role in many environments regardless of sulfate aerosol concentrations.

622

623   **Acknowledgements**

Atmospheric
Chemistry
and Physics
Discussions

Open Access

EGU

631   thank the Southern Oxidant and Aerosol Study (SOAS) science team, especially J.L. Jimenez

632   (CU Boulder) and A.G. Carlton (Rutgers) for facilitating our participation.

633
634
635
636
637
638
639
640
641
642
643
644
645
646
647
648
649
650
651
652
653
654
655
656
657
658
659
660
661
662
663
664
665
666
667
668
669
670
671
672
673
674

References

Attwood, A. R., R. A. Washenfelder, C. A. Brock, W. Hu, K. Baumann, P. Campuzano-Jost, D. A. Day, E. S. Edgerton, D. M. Murphy, B. B. Palm, A. McComiskey, N. L. Wagner, S. S. de Sa, A. Ortega, S. T. Martin, J. L. Jimenez, and S. S. Brown (2014), Trends in sulfate and organic aerosol mass in the Southeast U.S.: Impact on aerosol optical depth and radiative forcing, *Geophys. Res. Lett.*, *41*(21), 7701-7709, doi: 10.1002/2014gl061669.

Baasandorj, M., D. K. Papanastasiou, R. K. Talukdar, A. S. Hasson, and J. B. Burkholder (2010), (CH3)(3)COOH (tert-butyl hydroperoxide): OH reaction rate coefficients between 206 and 375 K and the OH photolysis quantum yield at 248 nm, *Phys. Chem. Chem. Phys.*, *12*(38), 12101-12111, doi: 10.1039/c0cp00463d.

Budisulistiorini, S. H., X. Li, S. T. Bairai, J. Renfro, Y. Liu, Y. J. Liu, K. A. McKinney, S. T. Martin, V. F. McNeill, H. O. T. Pye, A. Nenes, M. E. Neff, E. A. Stone, S. Mueller, C. Knote, S. L. Shaw, Z. Zhang, A. Gold, and J. D. Surratt (2015), Examining the effects of anthropogenic emissions on isoprene-derived secondary organic aerosol formation during the 2013 Southern Oxidant and Aerosol Study (SOAS) at the Look Rock, Tennessee ground site, *Atmospheric Chemistry and Physics*, *15*(15), 8871-8888, doi: 10.5194/acp-15-8871-2015.

Capouet, M., and J. F. Muller (2006), A group contribution method for estimating the vapour pressures of alpha-pinene oxidation products, *Atmospheric Chemistry and Physics*, *6*, 1455-1467.

Claeys, M., B. Graham, G. Vas, W. Wang, R. Vermeylen, V. Pashynska, J. Cafmeyer, P. Guyon, M. O. Andreae, P. Artaxo, and W. Maenhaut (2004), Formation of secondary organic aerosols through photooxidation of isoprene, *Science*, *303*(5661), 1173-1176, doi: 10.1126/science.1092805.

Compernolle, S., K. Ceulemans, and J. F. Muller (2011), EVAPORATION: a new vapour pressure estimation methodfor organic molecules including non-additivity and intramolecular interactions, *Atmospheric Chemistry and Physics*, *11*(18), 9431-9450, doi: 10.5194/acp-11-9431-2011.

Davison, B., R. Taipale, B. Langford, P. Misztal, S. Fares, G. Matteucci, F. Loreto, J. N. Cape, J. Rinne, and C. N. Hewitt (2009), Concentrations and fluxes of biogenic volatile organic compounds above a Mediterranean macchia ecosystem in western Italy, *Biogeosciences*, *6*(8), 1655-1670, doi: 10.5194/bg-6-1655-2009.

de Arellano, J. V. G., E. G. Patton, T. Karl, K. van den Dries, M. C. Barth, and J. J. Orlando (2011), The role of boundary layer dynamics on the diurnal evolution of isoprene and the hydroxyl radical over tropical forests, *J. Geophys. Res.-Atmos.*, *116*, doi: 10.1029/2010jd014857.

Ding, X., M. Zheng, L. P. Yu, X. L. Zhang, R. J. Weber, B. Yan, A. G. Russell, E. S. Edgerton, and X. M. Wang (2008), Spatial and seasonal trends in biogenic secondary organic aerosol tracers and water-soluble organic carbon in the southeastern United States, *Environmental science & technology*, *42*(14), 5171-5176, doi: 10.1021/es7032636.

Docherty, K. S., W. Wu, Y. B. Lim, and P. J. Ziemann (2005), Contributions of organic peroxides to secondary aerosol formed from reactions of monoterpenes with O-3, *Environmental science & technology*, *39*(11), 4049-4059, doi: 10.1021/es050228s.

Dommen, J., A. Metzger, J. Duplissy, M. Kalberer, M. R. Alfarra, A. Gascho, E. Weingartner, A. S. H. Prevot, B. Verheggen, and U. Baltensperger (2006), Laboratory observation of oligomers in the aerosol from isoprene/NOx photooxidation, *Geophys. Res. Lett.*, *33*(13), doi: 10.1029/2006gl026523.

Donahue, N. M., E. R. Trump, J. R. Pierce, and I. Riipinen (2011), Theoretical constraints on pure vapor-pressure driven condensation of organics to ultrafine particles, *Geophys. Res. Lett.*, *38*, doi: 10.1029/2011gl048115.

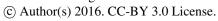Atmospheric
Chemistry
and Physics
Discussions
Open Access

EGU

722 Edney, E. O., T. E. Kleindienst, M. Jaoui, M. Lewandowski, J. H. Offenberg, W. Wang, and M. Claeys
723   (2005), Formation of 2-methyl tetrols and 2-methylglyceric acid in secondary organic aerosol
724   from laboratory irradiated isoprene/NO(X)/SO(2)/air mixtures and their detection in ambient
725   PM(2.5) samples collected in the eastern United States, *Atmospheric Environment*, *39*(29),
726   5281-5289, doi: 10.1016/j.atmosenv.2005.05.031.
727 Fuentes, J. D., D. Wang, and L. Gu (1999), Seasonal variations in isoprene emissions from a boreal
728   aspen forest, *J. Appl. Meteorol.*, *38*(7), 855-869, doi: 10.1175/1520-
729   0450(1999)038<0855:sviief>2.0.co;2.
730 Gaston, C. J., T. P. Riedel, Z. F. Zhang, A. Gold, J. D. Surratt, and J. A. Thornton (2014), Reactive Uptake
731   of an Isoprene-Derived Epoxydiol to Submicron Aerosol Particles, *Environmental science &
732   technology*, *48*(19), 11178-11186, doi: 10.1021/es5034266.
733 Gaston, C. J., F. D. Lopez-Hilfiker, L. E. Whybrew, O. Hadley, F. McNair, H. Gao, D. A. Jaffe, and J. A.
734   Thornton (2016), Online molecular characterization of fine particulate matter in Port Angeles,
735   WA: Evidence for a major impact from residential wood smoke, *Atmospheric Environment*,
736   *138*, 99-107, doi: 0.1016/j.atmosenv.2016.05.013.
737 Guenther, A. B., X. Jiang, C. L. Heald, T. Sakulyanontvittaya, T. Duhl, L. K. Emmons, and X. Wang
738   (2012), The Model of Emissions of Gases and Aerosols from Nature version 2.1 (MEGAN2.1):
739   an extended and updated framework for modeling biogenic emissions, *Geosci. Model Dev.*,
740   *5*(6), 1471-1492, doi: 10.5194/gmd-5-1471-2012.
741 Holzinger, R., E. Sanhueza, R. von Kuhlmann, B. Kleiss, L. Donoso, and P. J. Crutzen (2002), Diurnal
742   cycles and seasonal variation of isoprene and its oxidation products in the tropical savanna
743   atmosphere, *Glob. Biogeochem. Cycle*, *16*(4), doi: 10.1029/2001gb001421.
744 Hsieh, S., R. Vushe, Y. M. T. Tun, and J. L. Vallejo (2014), Trends in organic hydroperoxide
745   photodissociation and absorption cross sections between 266 and 377 nm, *Chem. Phys. Lett.*,
746   *591*, 99-102, doi: 10.1016/j.cplett.2013.11.008.
747 Hu, W. W., P. Campuzano-Jost, B. B. Palm, D. A. Day, A. M. Ortega, P. L. Hayes, J. E. Krechmer, Q.
748   Chen, M. Kuwata, Y. J. Liu, S. S. de Sa, K. McKinney, S. T. Martin, M. Hu, S. H. Budisulistiorini,
749   M. Riva, J. D. Surratt, J. M. St Clair, G. Isaacman-Van Wertz, L. D. Yee, A. H. Goldstein, S.
750   Carbone, J. Brito, P. Artaxo, J. A. de Gouw, A. Koss, A. Wisthaler, T. Mikoviny, T. Karl, L. Kaser,
751   W. Jud, A. Hansel, K. S. Docherty, M. L. Alexander, N. H. Robinson, H. Coe, J. D. Allan, M. R.
752   Canagaratna, F. Paulot, and J. L. Jimenez (2015), Characterization of a real-time tracer for
753   isoprene epoxydiols-derived secondary organic aerosol (IEPOX-SOA) from aerosol mass
754   spectrometer measurements, *Atmospheric Chemistry and Physics*, *15*(20), 11807-11833, doi:
755   10.5194/acp-15-11807-2015.
756 Jang, M. S., N. M. Czoschke, S. Lee, and R. M. Kamens (2002), Heterogeneous atmospheric aerosol
757   production by acid-catalyzed particle-phase reactions, *Science*, *298*(5594), 814-817, doi:
758   10.1126/science.1075798.
759 Jathar, S. H., C. D. Cappa, A. S. Wexler, J. H. Seinfeld, and M. J. Kleeman (2016), Simulating secondary
760   organic aerosol in a regional air quality model using the statistical oxidation model - Part 1:
761   Assessing the influence of constrained multi-generational ageing, *Atmospheric Chemistry and
762   Physics*, *16*(4), 2309-2322, doi: 10.5194/acp-16-2309-2016.
763 Jimenez, J. L., M. R. Canagaratna, N. M. Donahue, A. S. H. Prevot, Q. Zhang, J. H. Kroll, P. F. DeCarlo, J.
764   D. Allan, H. Coe, N. L. Ng, A. C. Aiken, K. S. Docherty, I. M. Ulbrich, A. P. Grieshop, A. L.
765   Robinson, J. Duplissy, J. D. Smith, K. R. Wilson, V. A. Lanz, C. Hueglin, Y. L. Sun, J. Tian, A.
766   Laaksonen, T. Raatikainen, J. Rautiainen, P. Vaattovaara, M. Ehn, M. Kulmala, J. M. Tomlinson,
767   D. R. Collins, M. J. Cubison, E. J. Dunlea, J. A. Huffman, T. B. Onasch, M. R. Alfarra, P. I.
768   Williams, K. Bower, Y. Kondo, J. Schneider, F. Drewnick, S. Borrmann, S. Weimer, K.
769   Demerjian, D. Salcedo, L. Cottrell, R. Griffin, A. Takami, T. Miyoshi, S. Hatakeyama, A.

Shimono, J. Y. Sun, Y. M. Zhang, K. Dzepina, J. R. Kimmel, D. Sueper, J. T. Jayne, S. C. Herndon, A. M. Trimborn, L. R. Williams, E. C. Wood, A. M. Middlebrook, C. E. Kolb, U. Baltensperger, and D. R. Worsnop (2009), Evolution of Organic Aerosols in the Atmosphere, *Science*, *326*(5959), 1525-1529, doi: 10.1126/science.1180353.

Kalogridis, C., V. Gros, R. Sarda-Esteve, B. Langford, B. Loubet, B. Bonsang, N. Bonnaire, E. Nemitz, A. C. Genard, C. Boissard, C. Fernandez, E. Ormeno, D. Baisnee, I. Reiter, and J. Lathiere (2014), Concentrations and fluxes of isoprene and oxygenated VOCs at a French Mediterranean oak forest, *Atmos. Chem. Phys.*, *14*(18), 10085-10102, doi: 10.5194/acp-14-10085-2014.

King, S. M., T. Rosenoern, J. E. Shilling, Q. Chen, Z. Wang, G. Biskos, K. A. McKinney, U. Poschl, and S. T. Martin (2010), Cloud droplet activation of mixed organic-sulfate particles produced by the photooxidation of isoprene, *Atmospheric Chemistry and Physics*, *10*(8), 3953-3964.

Kirkby, J., J. Duplissy, K. Sengupta, C. Frege, H. Gordon, C. Williamson, M. Heinritzi, M. Simon, C. Yan, J. Almeida, J. Trostl, T. Nieminen, I. K. Ortega, R. Wagner, A. Adamov, A. Amorim, A. K. Bernhammer, F. Bianchi, M. Breitenlechner, S. Brilke, X. M. Chen, J. Craven, A. Dias, S. Ehrhart, R. C. Flagan, A. Franchin, C. Fuchs, R. Guida, J. Hakala, C. R. Hoyle, T. Jokinen, H. Junninen, J. Kangasluoma, J. Kim, M. Krapf, A. Kurten, A. Laaksonen, K. Lehtipalo, V. Makhmutov, S. Mathot, U. Molteni, A. Onnela, O. Perakyla, F. Piel, T. Petaja, A. P. Praplan, K. Pringle, A. Rap, N. A. D. Richards, I. Riipinen, M. P. Rissanen, L. Rondo, N. Sarnela, S. Schobesberger, C. E. Scott, J. H. Seinfeld, M. Sipila, G. Steiner, Y. Stozhkov, F. Stratmann, A. Tome, A. Virtanen, A. L. Vogel, A. C. Wagner, P. E. Wagner, E. Weingartner, D. Wimmer, P. M. Winkler, P. L. Ye, X. Zhang, A. Hansel, J. Dommen, N. M. Donahue, D. R. Worsnop, U. Baltensperger, M. Kulmala, K. S. Carslaw, and J. Curtius (2016), Ion-induced nucleation of pure biogenic particles, *Nature*, *533*(7604), 521-+, doi: 10.1038/nature17953.

Kleindienst, T. E., M. Lewandowski, J. H. Offenberg, M. Jaoui, and E. O. Edney (2009), The formation of secondary organic aerosol from the isoprene plus OH reaction in the absence of NOx, *Atmospheric Chemistry and Physics*, *9*(17), 6541-6558.

Kourtchev, I., T. Ruuskanen, W. Maenhaut, M. Kulmala, and M. Claeys (2005), Observation of 2-methyltetrols and related photo-oxidation products of isoprene in boreal forest aerosols from Hyytiala, Finland, *Atmospheric Chemistry and Physics*, *5*, 2761-2770.

Krechmer, J. E., M. M. Coggon, P. Massoli, T. B. Nguyen, J. D. Crounse, W. W. Hu, D. A. Day, G. S. Tyndall, D. K. Henze, J. C. Rivera-Rios, J. B. Nowak, J. R. Kimmel, R. L. Mauldin, H. Stark, J. T. Jayne, M. Sipila, H. Junninen, J. M. S. Clair, X. Zhang, P. A. Feiner, L. Zhang, D. O. Miller, W. H. Brune, F. N. Keutsch, P. O. Wennberg, J. H. Seinfeld, D. R. Worsnop, J. L. Jimenez, and M. R. Canagaratna (2015), Formation of Low Volatility Organic Compounds and Secondary Organic Aerosol from Isoprene Hydroxyhydroperoxide Low-NO Oxidation, *Environmental science & technology*, *49*(17), 10330-10339, doi: 10.1021/acs.est.5b02031.

Kroll, J. H., N. L. Ng, S. M. Murphy, R. C. Flagan, and J. H. Seinfeld (2005), Secondary organic aerosol formation from isoprene photooxidation under high-NOx conditions, *Geophys. Res. Lett.*, *32*(18), doi: 10.1029/2005gl023637.

Kroll, J. H., N. L. Ng, S. M. Murphy, R. C. Flagan, and J. H. Seinfeld (2006), Secondary organic aerosol formation from isoprene photooxidation, *Environmental science & technology*, *40*(6), 1869-1877, doi: 10.1021/es0524301.

Kurten, T., K. Tiusanen, P. Roldin, M. Rissanen, J. N. Luy, M. Boy, M. Ehn, and N. Donahue (2016), alpha-Pinene Autoxidation Products May Not Have Extremely Low Saturation Vapor Pressures Despite High O:C Ratios, *J. Phys. Chem. A*, *120*(16), 2569-2582, doi: 10.1021/acs.jpca.6b02196.

Lane, T. E., N. M. Donahue, and S. N. Pandis (2008), Effect of NO(x) on secondary organic aerosol concentrations, *Environmental science & technology*, *42*(16), 6022-6027, doi: 10.1021/es703225a.

Atmospheric
Chemistry
and Physics
Discussions

Open Access

EGU

818   Lee, B. H., F. D. Lopez-Hilfiker, C. Mohr, T. Kurten, D. R. Worsnop, and J. A. Thornton (2014), An iodide-
819   adduct high-resolution time-of-flight chemical-ionization mass spectrometer: application to
820   atmospheric inorganic and organic compounds, *Environmental science & technology*, *48*(11),
821   6309-6317, doi: 10.1021/es500362a.
822   Lee, B. H., C. Mohr, F. D. Lopez-Hilfiker, A. Lutz, M. Hallquist, L. Lee, P. Romer, R. C. Cohen, S. Iyer, T.
823   Kurtén, W. Hu, D. A. Day, P. Campuzano-Jost, J. L. Jimenez, L. Xu, N. L. Ng, H. Guo, R. J. Weber,
824   R. J. Wild, S. S. Brown, A. Koss, J. de Gouw, K. Olson, A. H. Goldstein, R. Seco, S. Kim, K.
825   McAvey, P. B. Shepson, T. Starn, K. Baumann, E. S. Edgerton, J. Liu, J. E. Shilling, D. O. Miller,
826   W. Brune, S. Schobesberger, E. L. D'Ambro, and J. A. Thornton (2016), Highly functionalized
827   organic nitrates in the southeast United States: Contribution to secondary organic aerosol and
828   reactive nitrogen budgets, *Proceedings of the National Academy of Sciences*, doi:
829   10.1073/pnas.1508108113.
830   Lee, B. S., and J. L. Wang (2006), Concentration variation of isoprene and its implications for peak
831   ozone   concentration,   *Atmos.   Environ.*,   *40*(28),   5486-5495,   doi:
832   10.1016/j.atmosenv.2006.03.035.
833   Lin, Y. H., E. M. Knipping, E. S. Edgerton, S. L. Shaw, and J. D. Surratt (2013a), Investigating the
834   influences of SO2 and NH3 levels on isoprene-derived secondary organic aerosol formation
835   using conditional sampling approaches, *Atmospheric Chemistry and Physics*, *13*(16), 8457-
836   8470, doi: 10.5194/acp-13-8457-2013.
837   Lin, Y. H., H. Budisulistiorini, K. Chu, R. A. Siejack, H. F. Zhang, M. Riva, Z. F. Zhang, A. Gold, K. E.
838   Kautzman, and J. D. Surratt (2014), Light-Absorbing Oligomer Formation in Secondary Organic
839   Aerosol from Reactive Uptake of Isoprene Epoxydiols, *Environmental science & technology*,
840   *48*(20), 12012-12021, doi: 10.1021/es503142b.
841   Lin, Y. H., Z. F. Zhang, K. S. Docherty, H. F. Zhang, S. H. Budisulistiorini, C. L. Rubitschun, S. L. Shaw, E.
842   M. Knipping, E. S. Edgerton, T. E. Kleindienst, A. Gold, and J. D. Surratt (2012), Isoprene
843   Epoxydiols as Precursors to Secondary Organic Aerosol Formation: Acid-Catalyzed Reactive
844   Uptake Studies with Authentic Compounds, *Environmental science & technology*, *46*(1), 250-
845   258, doi: 10.1021/es202554c.
846   Lin, Y. H., H. F. Zhang, H. O. T. Pye, Z. F. Zhang, W. J. Marth, S. Park, M. Arashiro, T. Q. Cui, H.
847   Budisulistiorini, K. G. Sexton, W. Vizuete, Y. Xie, D. J. Luecken, I. R. Piletic, E. O. Edney, L. J.
848   Bartolotti, A. Gold, and J. D. Surratt (2013b), Epoxide as a precursor to secondary organic
849   aerosol formation from isoprene photooxidation in the presence of nitrogen oxides, *Proc.
850   Natl. Acad. Sci. U. S. A.*, *110*(17), 6718-6723, doi: 10.1073/pnas.1221150110.
851   Liu, J. M. (2016), Efficient Organic Aerosol Formation From Isoprene Photooxidation in Pristine
852   Conditions, *Environmental science & technology*, *under review*.
853   Liu, S., J. E. Shilling, C. Song, N. Hiranuma, R. A. Zaveri, and L. M. Russell (2012), Hydrolysis of
854   Organonitrate Functional Groups in Aerosol Particles, *Aerosol Sci. Technol.*, *46*(12), 1359-1369,
855   doi: 10.1080/02786826.2012.716175.
856   Liu, Y., M. Kuwata, B. F. Strick, F. M. Geiger, R. J. Thomson, K. A. McKinney, and S. T. Martin (2014),
857   Uptake of Epoxydiol Isomers Accounts for Half of the Particle-Phase Material Produced from
858   Isoprene Photooxidation via the HO Pathway, *Environmental science & technology*, doi:
859   10.1021/es5034298.
860   Lopez-Hilfiker, F. D., S. Iyer, C. Mohr, B. H. Lee, E. L. D'Ambro, T. Kurten, and J. A. Thornton (2016a),
861   Constraining the sensitivity of iodide adduct chemical ionization mass spectrometry to
862   multifunctional organic molecules using the collision limit and thermodynamic stability of
863   iodide ion adducts, *Atmospheric Measurement Techniques*, *9*(4), 1505-1512, doi: 10.5194/amt-
864   9-1505-2016.

Atmospheric
Chemistry
and Physics
Discussions

Lopez-Hilfiker, F. D., C. Mohr, M. Ehn, F. Rubach, E. Kleist, J. Wildt, T. F. Mentel, A. Lutz, M. Hallquist, D. Worsnop, and J. A. Thornton (2014), A novel method for online analysis of gas and particle composition: description and evaluation of a Filter Inlet for Gases and AEROsols (FIGAERO), *Atmospheric Measurement Techniques*, *7*(4), 983-1001, doi: 10.5194/amt-7-983-2014.

Lopez-Hilfiker, F. D., C. Mohr, M. Ehn, F. Rubach, E. Kleist, J. Wildt, T. F. Mentel, A. J. Carrasquillo, K. E. Daumit, J. F. Hunter, J. H. Kroll, D. R. Worsnop, and J. A. Thornton (2015), Phase partitioning and volatility of secondary organic aerosol components formed from alpha-pinene ozonolysis and OH oxidation: the importance of accretion products and other low volatility compounds, *Atmospheric Chemistry and Physics*, *15*(14), 7765-7776, doi: 10.5194/acp-15-7765-2015.

Lopez-Hilfiker, F. D., C. Mohr, E. L. D'Ambro, A. Lutz, T. P. Riedel, C. J. Gaston, S. Iyer, Z. Zhang, A. Gold, J. D. Surratt, B. H. Lee, T. Kurten, W. W. Hu, J. Jimenez, M. Hallquist, and J. A. Thornton (2016b), Molecular Composition and Volatility of Organic Aerosol in the Southeastern US: Implications for IEPOX Derived SOA, *Environmental science & technology*, *50*(5), 2200-2209, doi: 10.1021/acs.est.5b04769.

Nannoolal, Y., J. Rarey, and D. Ramjugernath (2008), Estimation of pure component properties - Part 3. Estimation of the vapor pressure of non-electrolyte organic compounds via group contributions and group interactions, *Fluid Phase Equilib.*, *269*(1-2), 117-133, doi: 10.1016/j.fluid.2008.04.020.

Nguyen, T. B., M. M. Coggon, K. H. Bates, X. Zhang, R. H. Schwantes, K. A. Schilling, C. L. Loza, R. C. Flagan, P. O. Wennberg, and J. H. Seinfeld (2014), Organic aerosol formation from the reactive uptake of isoprene epoxydiols (IEPOX) onto non-acidified inorganic seeds, *Atmospheric Chemistry and Physics*, *14*(7), 3497-3510, doi: 10.5194/acp-14-3497-2014.

Pandis, S. N., S. E. Paulson, J. H. Seinfeld, and R. C. Flagan (1991), Aerosol formation in the photooxidation of isoprene and beta-pinene, *Atmospheric Environment Part a-General Topics*, *25*(5-6), 997-1008, doi: 10.1016/0960-1686(91)90141-s.

Pankow, J. F. (1994), AN ABSORPTION-MODEL OF GAS-PARTICLE PARTITIONING OF ORGANIC-COMPOUNDS IN THE ATMOSPHERE, *Atmospheric Environment*, *28*(2), 185-188, doi: 10.1016/1352-2310(94)90093-0.

Pankow, J. F., and W. E. Asher (2008), SIMPOL.1: a simple group contribution method for predicting vapor pressures and enthalpies of vaporization of multifunctional organic compounds, *Atmospheric Chemistry and Physics*, *8*(10), 2773-2796.

Paulot, F., J. D. Crounse, H. G. Kjaergaard, J. H. Kroll, J. H. Seinfeld, and P. O. Wennberg (2009a), Isoprene photooxidation: new insights into the production of acids and organic nitrates, *Atmospheric Chemistry and Physics*, *9*(4), 1479-1501.

Paulot, F., J. D. Crounse, H. G. Kjaergaard, A. Kurten, J. M. St Clair, J. H. Seinfeld, and P. O. Wennberg (2009b), Unexpected Epoxide Formation in the Gas-Phase Photooxidation of Isoprene, *Science*, *325*(5941), 730-733, doi: 10.1126/science.1172910.

Poschl, U. (2005), Atmospheric aerosols: Composition, transformation, climate and health effects, *Angew. Chem.-Int. Edit.*, *44*(46), 7520-7540, doi: 10.1002/anie.200501122.

Riipinen, I., J. R. Pierce, T. Yli-Juuti, T. Nieminen, S. Hakkinen, M. Ehn, H. Junninen, K. Lehtipalo, T. Petaja, J. Slowik, R. Chang, N. C. Shantz, J. Abbatt, W. R. Leaitch, V. M. Kerminen, D. R. Worsnop, S. N. Pandis, N. M. Donahue, and M. Kulmala (2011), Organic condensation: a vital link connecting aerosol formation to cloud condensation nuclei (CCN) concentrations, *Atmospheric Chemistry and Physics*, *11*(8), 3865-3878, doi: 10.5194/acp-11-3865-2011.

Rinne, H. J. I., A. B. Guenther, J. P. Greenberg, and P. C. Harley (2002), Isoprene and monoterpene fluxes measured above Amazonian rainforest and their dependence on light and temperature, *Atmos. Environ.*, *36*(14), 2421-2426, doi: 10.1016/s1352-2310(01)00523-4.

Atmospheric
Chemistry
and Physics
Discussions

912   **Riva, M., H. Budisulistiorini, Y. Chen, Z. Zhang, E. L. D'Ambro, X. Zhang, A. Gold, B. J. Turpin, J. A.**
913   **Thornton, M. Canagaratna, and J. Surratt (2016), Chemical Characterization of Secondary**
914   **Organic Aerosol from Oxidation of Isoprene Hydroxyhydroperoxides** *Environmental science &*
915   *technology*, *Under Review*.
916   **Roehl, C. M., Z. Marka, J. L. Fry, and P. O. Wennberg (2007), Near-UV photolysis cross sections of**
917   **CH3OOH and HOCH2OOH determined via action spectroscopy,** *Atmospheric Chemistry and*
918   *Physics*, *7*, 713-720.
919   **Sato, K., S. Nakao, C. H. Clark, L. Qi, and D. R. Cocker (2011), Secondary organic aerosol formation from**
920   **the photooxidation of isoprene, 1,3-butadiene, and 2,3-dimethyl-1,3-butadiene under high**
921   **NOx conditions,** *Atmospheric Chemistry and Physics*, *11*(14), 7301-7317, doi: 10.5194/acp-11-
922   7301-2011.
923   **Shilling, J. E., Q. Chen, S. M. King, T. Rosenoern, J. H. Kroll, D. R. Worsnop, K. A. McKinney, and S. T.**
924   **Martin (2008), Particle mass yield in secondary organic aerosol formed by the dark ozonolysis**
925   **of alpha-pinene,** *Atmospheric Chemistry and Physics*, *8*(7), 2073-2088, doi: 10.5194/acp-8-
926   2073-2008.
927   **Shilling, J. E., R. A. Zaveri, J. D. Fast, L. Kleinman, M. L. Alexander, M. R. Canagaratna, E. Fortner, J. M.**
928   **Hubbe, J. T. Jayne, A. Sedlacek, A. Setyan, S. Springston, D. R. Worsnop, and Q. Zhang (2013),**
929   **Enhanced SOA formation from mixed anthropogenic and biogenic emissions during the CARES**
930   **campaign,** *Atmospheric Chemistry and Physics*, *13*(4), 2091-2113, doi: 10.5194/acp-13-2091-
931   2013.
932   **St Clair, J. M., J. C. Rivera-Rios, J. D. Crounse, H. C. Knap, K. H. Bates, A. P. Teng, S. Jorgensen, H. G.**
933   **Kjaergaard, F. N. Keutsch, and P. O. Wennberg (2016), Kinetics and Products of the Reaction of**
934   **the First-Generation Isoprene Hydroxy Hydroperoxide (ISOPOOH) with OH,** *J. Phys. Chem. A*,
935   *120*(9), 1441-1451, doi: 10.1021/acs.jpca.5b06532.
936   **Surratt, J. D., M. Lewandowski, J. H. Offenberg, M. Jaoui, T. E. Kleindienst, E. O. Edney, and J. H.**
937   **Seinfeld (2007), Effect of acidity on secondary organic aerosol formation from isoprene,**
938   *Environmental science & technology*, *41*(15), 5363-5369, doi: 10.1021/es0704176.
939   **Surratt, J. D., A. W. H. Chan, N. C. Eddingsaas, M. N. Chan, C. L. Loza, A. J. Kwan, S. P. Hersey, R. C.**
940   **Flagan, P. O. Wennberg, and J. H. Seinfeld (2010), Reactive intermediates revealed in**
941   **secondary organic aerosol formation from isoprene,** *Proc. Natl. Acad. Sci. U. S. A.*, *107*(15),
942   6640-6645, doi: 10.1073/pnas.0911114107.
943   **Surratt, J. D., S. M. Murphy, J. H. Kroll, N. L. Ng, L. Hildebrandt, A. Sorooshian, R. Szmigielski, R.**
944   **Vermeylen, W. Maenhaut, M. Claeys, R. C. Flagan, and J. H. Seinfeld (2006), Chemical**
945   **composition of secondary organic aerosol formed from the photooxidation of isoprene,** *J.*
946   *Phys. Chem. A*, *110*(31), 9665-9690, doi: 10.1021/jp061734m.
947   **Tsai, I. C., J. P. Chen, C. S. C. Lung, N. Li, W. N. Chen, T. M. Fu, C. C. Chang, and G. D. Hwang (2015),**
948   **Sources and formation pathways of organic aerosol in a subtropical metropolis during**
949   **summer,** *Atmospheric Environment*, *117*, 51-60, doi: 10.1016/j.atmosenv.2015.07.005.
950   **Valorso, R., B. Aumont, M. Camredon, T. Raventos-Duran, C. Mouchel-Vallon, N. L. Ng, J. H. Seinfeld, J.**
951   **Lee-Taylor, and S. Madronich (2011), Explicit modelling of SOA formation from alpha-pinene**
952   **photooxidation: sensitivity to vapour pressure estimation,** *Atmospheric Chemistry and*
953   *Physics*, *11*(14), 6895-6910, doi: 10.5194/acp-11-6895-2011.
954   **Washenfelder, R. A., A. R. Attwood, C. A. Brock, H. Guo, L. Xu, R. J. Weber, N. L. Ng, H. M. Allen, B. R.**
955   **Ayres, K. Baumann, R. C. Cohen, D. C. Draper, K. C. Duffey, E. Edgerton, J. L. Fry, W. W. Hu, J. L.**
956   **Jimenez, B. B. Palm, P. Romer, E. A. Stone, P. J. Wooldridge, and S. S. Brown (2015), Biomass**
957   **burning dominates brown carbon absorption in the rural southeastern United States,**
958   *Geophys. Res. Lett.*, *42*(2), 653-664, doi: 10.1002/2014gl062444.

959   Weber, R. J., A. P. Sullivan, R. E. Peltier, A. Russell, B. Yan, M. Zheng, J. de Gouw, C. Warneke, C. Brock,
960   J. S. Holloway, E. L. Atlas, and E. Edgerton (2007), A study of secondary organic aerosol
961   formation in the anthropogenic-influenced southeastern United States, *J. Geophys. Res.-*
962   *Atmos.*, *112*(D13), doi: 10.1029/2007jd008408.
963   Xia, X., and P. K. Hopke (2006), Seasonal variation of 2-methyltetrols in ambient air samples,
964   *Environmental science & technology*, *40*(22), 6934-6937, doi: 10.1021/es060988l.
965   Xu, L., M. S. Kollman, C. Song, J. E. Shilling, and N. L. Ng (2014), Effects of NOx on the volatility of
966   secondary organic aerosol from isoprene photooxidation, *Environmental science &*
967   *technology*, *48*(4), 2253-2262, doi: 10.1021/es404842g.
968   Xu, L., H. Y. Guo, C. M. Boyd, M. Klein, A. Bougiatioti, K. M. Cerully, J. R. Hite, G. Isaacman-VanWertz,
969   N. M. Kreisberg, C. Knote, K. Olson, A. Koss, A. H. Goldstein, S. V. Hering, J. de Gouw, K.
970   Baumann, S. H. Lee, A. Nenes, R. J. Weber, and N. L. Ng (2015), Effects of anthropogenic
971   emissions on aerosol formation from isoprene and monoterpenes in the southeastern United
972   States, *Proc. Natl. Acad. Sci. U. S. A.*, *112*(1), 37-42, doi: 10.1073/pnas.1417609112.
973   Yang, K. L., C. C. Ting, J. L. Wang, O. W. Wingenter, and C. C. Chan (2005), Diurnal and seasonal cycles
974   of ozone precursors observed from continuous measurement at an urban site in Taiwan,
975   *Atmos. Environ.*, *39*(18), 3221-3230, doi: 10.1016/j.atmosenv.2005.02.003.
976   Zhang, H., J. D. Surratt, Y. H. Lin, J. Bapat, and R. M. Kamens (2011), Effect of relative humidity on SOA
977   formation from isoprene/NO photooxidation: enhancement of 2-methylglyceric acid and its
978   corresponding oligoesters under dry conditions, *Atmospheric Chemistry and Physics*, *11*(13),
979   6411-6424, doi: 10.5194/acp-11-6411-2011.
980   Zhang, Q., J. L. Jimenez, M. R. Canagaratna, J. D. Allan, H. Coe, I. Ulbrich, M. R. Alfarra, A. Takami, A.
981   M. Middlebrook, Y. L. Sun, K. Dzepina, E. Dunlea, K. Docherty, P. F. DeCarlo, D. Salcedo, T.
982   Onasch, J. T. Jayne, T. Miyoshi, A. Shimono, S. Hatakeyama, N. Takegawa, Y. Kondo, J.
983   Schneider, F. Drewnick, S. Borrmann, S. Weimer, K. Demerjian, P. Williams, K. Bower, R.
984   Bahreini, L. Cottrell, R. J. Griffin, J. Rautiainen, J. Y. Sun, Y. M. Zhang, and D. R. Worsnop
985   (2007), Ubiquity and dominance of oxygenated species in organic aerosols in
986   anthropogenically-influenced Northern Hemisphere midlatitudes, *Geophys. Res. Lett.*, *34*(13),
987   doi: 10.1029/2007gl029979.
988   Zhang, X., C. D. Cappa, S. H. Jathar, R. C. McVay, J. J. Ensberg, M. J. Kleeman, and J. H. Seinfeld (2014),
989   Influence of vapor wall loss in laboratory chambers on yields of secondary organic aerosol,
990   *Proc. Natl. Acad. Sci. U. S. A.*, *111*(16), 5802-5807, doi: 10.1073/pnas.1404727111.

991

992
993
994
995
996
997
998
999
1000
1001
1002
1003
1004

Atmospheric
Chemistry
and Physics
Discussions

Open Access

EGU

Figure and Table Captions

Table 1. Gas- and particle-phase compounds detailed in the mass spectra in Figure 2 (top). Many molecular compositions are observed in both the gas- and particle-phase. If the composition is observed in the particle phase, a T_{max} is listed at both low (0 ppb input NO) and high (20 ppb input NO) NO_x. The desorption shape is also listed and is consistent across NO_x conditions. The significance of the T_{max} and desorption shape are discussed in detail in the text. If the compound is only detected in the gas phase, "NA" is listed in the T_{max} and thermogram columns, indicating that those values are not applicable.

Figure 1. Overview of the 2014 and 2015 measurements taken at PNNL. The left column is data from the 2014 campaign, the right column is 2015. The top row shows gas-phase compounds measured by the PTR-MS and FIGAERO-CIMS, as well as input concentrations of H_2O_2, NO, and isoprene. Middle row shows the OA as measured by the AMS. Steady state periods are shown within magenta circles, AMS blanks as black squares. Select particle phase species measured by the FIGAERO-CIMS are in the bottom row. Grey shaded areas in each column indicate when chamber lights were off for chamber cleaning and a dark NO_3 experiment (in 2014) which is not discussed here. Note that the axis limits are not the same due to a wide range in concentrations across years, while $C_5H_{12}O_5$ has been enhanced 5x and $C_5H_{11}NO_7$ has been enhanced 20x in the bottom rows to clearly show the behavior of each species on the same axis.

Figure 2. Mass spectra for compounds with composition $C_xH_yO_zI^-$ (green) and $C_xH_yNO_zI^-$ (blue) at low (left) and high (right) NO input in both the gas- (top) and particle- (bottom) phases. Bars are sized by the square root of signal (counts s^{-1} for the gas-phase, counts for the particle-phase) to show the dynamic range. Major components are labeled with letters corresponding to those found in Table 1.

Figure 3. Top: Normalized signals of $C_5H_{12}O_6$ and $C_5H_{11}NO_7$, believed to originate in the gas phase from the same $C_5H_{11}O_6$ peroxy radical, as well as $C_5H_{12}O_5$, as a function of input NO. Signal is normalized to maximum signal for each compound to show the relative behaviors. Bottom: The mass fraction of organic nitrates as a function of NO. Mass fraction refers to the mass concentration of FIGAERO-CIMS measured OrgN relative to the total mass concentration of organics (non-nitrogen containing + OrgN) measured by the FIGAERO-CIMS.

Figure 4. Time evolution of particle-phase concentrations in a batch mode isoprene photochemical oxidation experiment at low-NO_x. Time increases from left to right and the size of the pies is proportional to the amount of OA present which is: 9.8, 15.0, 14.8, 14.6 µg/m^3 from left to right.

Figure 5. Top: Predicted versus measured fraction in the particle-phase (F_p). Predicted F_p is obtained from equation 1 where C^*s were calculated with the EVAPORATION group-contribution method [*Compernolle et al.*, 2011] labeled as "Group-Cont. C^*" in the bottom panels. Measured F_p is the direct measurement from the FIGAERO. Bottom: The F_p can also be predicted based on the calibrated FIGAERO temperature axis as discussed in the methods and is shown as the predicted F_p here. Agreement can be reached for two representative compounds where the F_p is over and correctly predicted (left, right respectively).

Atmospheric
Chemistry
and Physics
Discussions

Open Access

EGU

Figure 6. Top: Sum thermograms of α-pinene + O_3 compared to isoprene (C_5H_8) photooxidation with and without NO_x. The α-pinene sum thermogram has been reported previously (Lopez-Hilfiker et al. [2015], Fig 5). Bottom: The sum thermograms at low (left) and high (right) input NO. The thermogram of $C_5H_{12}O_6$, the largest signal in both cases, is separated out (dark green) and the sum of the remaining signal minus $C_5H_{12}O_6$ is displayed as the remaining signal (light green). At high NO input the sum of OrgN and the sum of non-nitrate organics are plotted (dashed lines, independent of solid lines) to show the relative thermogram features.

Figure 7. Top: Thermograms of $C_5H_{12}O_6$ observed during chamber experiments at PNNL (diamonds) compared to those measured during the SOAS field campaign (solid line). Bottom: Diurnal behavior of prominent C_5 compounds measured in the PNNL chamber and detected at SOAS: $C_5H_{12}O_6$, $C_5H_{12}O_5$, $C_5H_{10}O_6$, $C_5H_{10}O_5$, $C_5H_{11}NO_7$, and the sum of all 5. Arrows indicate which y-axis each compound is plotted on. The diurnal profile of these compounds maximizes during daylight hours and minimizes during the night as would be expected.
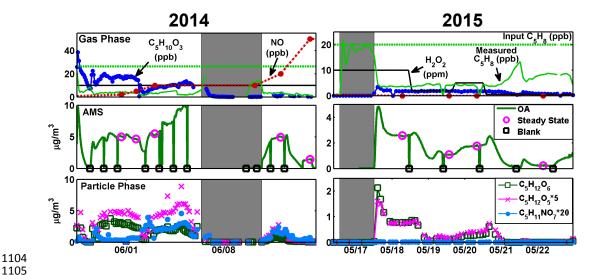
Atmospheric
Chemistry
and Physics
Discussions

Letter	Mass	Molecular Composition	Particle-phase T_{max}, Low NO$_x$	Particle-phase T_{max}, High NO$_x$	thermogram shape
a	172.9105	$CH_2O_2I^-$	87	94	broad
b	202.9211	$C_2H_4O_3I^-$	113	115	broad
c	216.9367	$C_3H_6O_3I^-$	76	100	broad
d	230.9524	$C_4H_8O_3I^-$	87	115	broad
e	244.968	$C_5H_{10}O_3I^-$	NA	NA	NA
f	258.9473	$C_5H_8O_4I^-$	76, 111	70, 115	double
g	275.9374	$C_4H_7NO_5I^-$	88	115	broad
h	289.9531	$C_5H_9NO_5I^-$	NA	NA	NA
i	305.948	$C_5H_9NO_6I^-$	NA	NA	NA
j	246.9473	$C_4H_8O_4I^-$	95	110	broad
k	278.9735	$C_5H_{12}O_5I^-$	60	48	Gaussian
l	294.9684	$C_5H_{12}O_6I^-$	63	56	Gaussian
m	323.9586	$C_5H_{11}NO_7I^-$	72	50	Gaussian
n	339.9535	$C_5H_{11}NO_8I^-$	53	45	Gaussian

Table 1. Gas- and particle-phase compounds detailed in the mass spectra in Figure 2 (top). Many molecular compositions are observed in both the gas- and particle-phase. If the composition is observed in the particle phase, a T_{max} is listed at both low (0 ppb input NO) and high (20 ppb input NO) NO$_x$. The desorption shape is also listed and is consistent across NO$_x$ conditions. The significance of the T_{max} and desorption shape are discussed in detail in the text. If the compound is only detected in the gas phase, "NA" is listed in the T_{max} and thermogram columns, indicating that those values are not applicable.

Atmospheric
Chemistry
and Physics
Discussions

EGU

Figure 1. Overview of the 2014 and 2015 measurements taken at PNNL. The left column is data from the 2014 campaign, the right column is 2015. The top row shows gas-phase compounds measured by the PTR-MS and FIGAERO-CIMS, as well as input concentrations of H_2O_2, NO, and isoprene. Middle row shows the OA as measured by the AMS. Steady state periods are shown within magenta circles, AMS blanks as black squares. Select particle phase species measured by the FIGAERO-CIMS are in the bottom row. Grey shaded areas in each column indicate when chamber lights were off for chamber cleaning and a dark NO_3 experiment (in 2014) which is not discussed here. Note that the axis limits are not the same due to a wide range in concentrations across years, while $C_5H_{12}O_5$ has been enhanced 5x and $C_5H_{11}NO_7$ has been enhanced 20x in the bottom rows to clearly show the behavior of each species on the same axis.
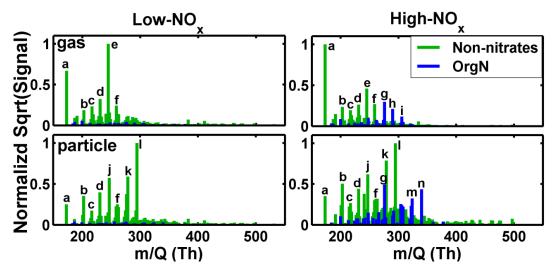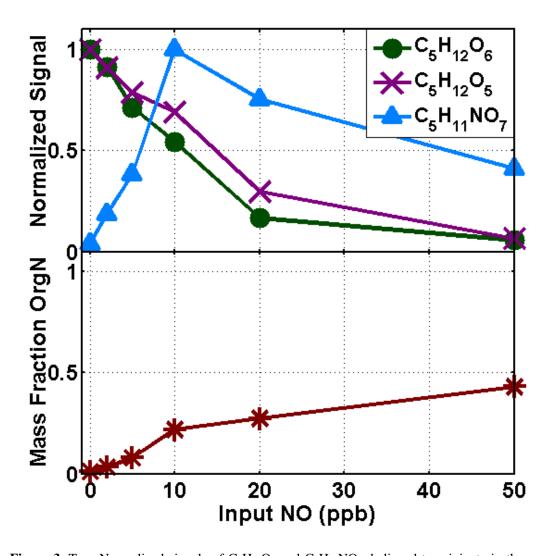
1120
1121
Figure 2. Mass spectra for compounds with composition $C_xH_yO_zI^-$ (green) and $C_xH_yNO_zI^-$ (blue)
at low (left) and high (right) NO input in both the gas- (top) and particle- (bottom) phases. Bars
are sized by the square root of signal (counts s^{-1} for the gas-phase, counts for the particle-phase)
to show the dynamic range. Major components are labeled with letters corresponding to those
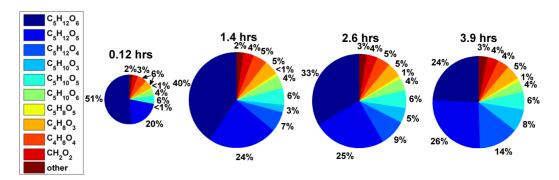found in Table 1.

Figure 3. Top: Normalized signals of $C_5H_{12}O_6$ and $C_5H_{11}NO_7$, believed to originate in the gas phase from the same $C_5H_{11}O_6$ peroxy radical, as well as $C_5H_{12}O_5$, as a function of input NO. Signal is normalized to maximum signal for each compound to show the relative behaviors. Bottom: The mass fraction of organic nitrates as a function of NO. Mass fraction refers to the mass concentration of FIGAERO-CIMS measured OrgN relative to the total mass concentration of organics (non-nitrogen containing + OrgN) measured by the FIGAERO-CIMS.
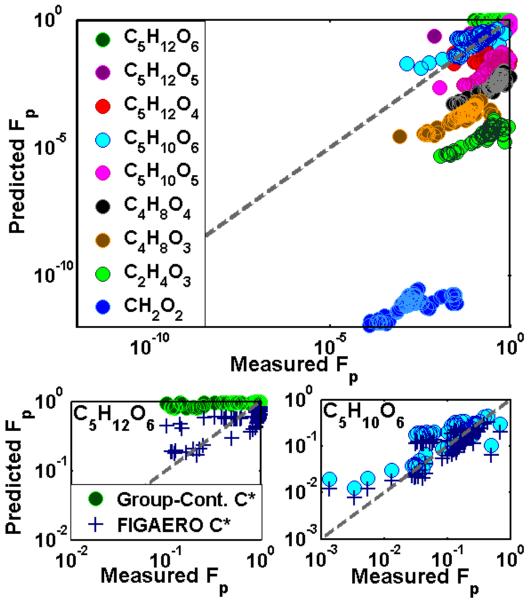
Atmospheric
Chemistry
and Physics
Discussions

Open Access

EGU

Figure 4. Time evolution of particle-phase concentrations in a batch mode isoprene photochemical oxidation experiment at low-NO$_x$. Time increases from left to right and the size of the pies is proportional to the amount of OA present which is: 9.8, 15.0, 14.8, 14.6 µg/m^3 from left to right.
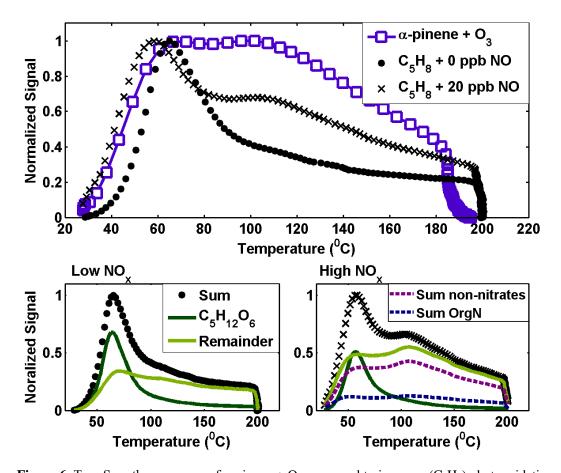
Figure 5. Top: Predicted versus measured fraction in the particle-phase (F_p). Predicted F_p is obtained from equation 1 where C^*s were calculated with the EVAPORATION group-contribution method [*Compernolle et al.*, 2011] labeled as "Group-Cont. C^*" in the bottom panels. Measured F_p is the direct measurement from the FIGAERO. Bottom: The F_p can also be predicted based on the calibrated FIGAERO temperature axis as discussed in the methods and is shown as the predicted F_p here. Agreement can be reached for two representative compounds where the F_p is over and correctly predicted (left, right respectively).
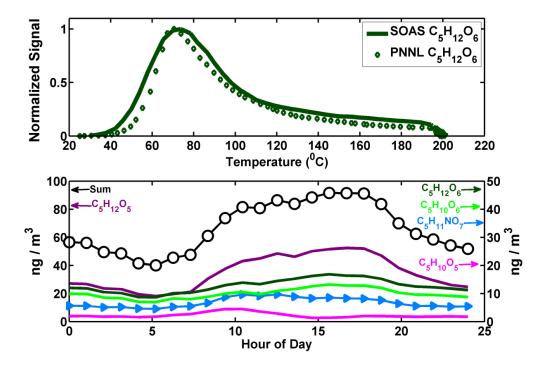
Figure 6. Top: Sum thermograms of α-pinene + O₃ compared to isoprene (C_5H_8) photooxidation with and without NO_x. The α-pinene sum thermogram has been reported previously (Lopez-Hilfiker et al. [2015], Fig 5). Bottom: The sum thermograms at low (left) and high (right) input NO. The thermogram of $C_5H_{12}O_6$, the largest signal in both cases, is separated out (dark green) and the sum of the remaining signal minus $C_5H_{12}O_6$ is displayed as the remaining signal (light green). At high NO input the sum of OrgN and the sum of non-nitrate organics are plotted (dashed lines, independent of solid lines) to show the relative thermogram features.

Atmospheric
Chemistry
and Physics
Discussions

Figure 7. Top: Thermograms of $C_5H_{12}O_6$ observed during chamber experiments at PNNL (diamonds) compared to those measured during the SOAS field campaign (solid line). Bottom: Diurnal behavior of prominent C_5 compounds measured in the PNNL chamber and detected at SOAS: $C_5H_{12}O_6$, $C_5H_{12}O_5$, $C_5H_{10}O_6$, $C_5H_{10}O_5$, $C_5H_{11}NO_7$, and the sum of all 5. Arrows indicate which y-axis each compound is plotted on. The diurnal profile of these compounds maximizes during daylight hours and minimizes during the night as would be expected.